

NANOINDENTATION OF PERI-IMPLANT BONE AND DENTIN

by

Allen Tang

B.A.Sc., University of British Columbia, Canada, 2003

A THESIS SUBMITTED IN PARTIAL FULFILLMENT OF
THE REQUIREMENTS FOR THE DEGREE OF

MASTER OF APPLIED SCIENCE

in

THE FACULTY OF GRADUATE STUDIES

(Materials Engineering)

THE UNIVERSITY OF BRITISH COLUMBIA

(Vancouver)

March 2008

© Allen Tang, 2008

ABSTRACT

Advances in the field of medicine have extended the average human life expectancy worldwide. As a result an increasing number of people will suffer from problems associated with their mineralized tissues and will require orthopedic and dental implants to restore their quality of life. Ideally, implants should have mechanical and structural properties compatible with the original mineralized tissue, and should also promote faster and stronger implant fixation. An improved understanding of the properties of mineralized tissues can help with the improvements of implants. This thesis focuses on improving the understanding of two aspects related to mineralized tissues and implant systems: the mechanical properties of peri-implant bone, and the mechanical, composition and structural properties of dentin and jawbone.

Studies have shown that local delivery of alendronate, an anti-osteoporosis drug, enhances new bone formation; however, the effects of the drug on the elastic modulus of new formed bone are unknown. In this study, nanoindentation was used to evaluate and compare the elastic modulus of peri-implant bone with and without the presence of alendronate. To better understand the properties of dentin and jawbone, nanoindentation and qualitative backscattered electron imaging were used to measure their elastic modulus, mineral content and volume fraction, and regression analyses were used to establish correlation between the properties.

In this thesis, mineralized tissue samples were collected from an animal study. To study the effects of alendronate on the elastic modulus of peri-implant bone, porous

tantalum implants with three different coating treatments were used: non-coated (Ta), calcium phosphate coated (Ta-CaP), alendronate-immobilized-calcium-phosphate coated (Ta-CaP-ALN). The calcium phosphate coatings, with or without alendronate, increased the elastic modulus of peri-implant Ingrown Bone by approximately 22% (3GPa). The addition of alendronate did not significantly increase the elastic modulus of peri-implant.

For the study of dentin and jawbone, regression analyses showed that the elastic modulus of dentin is strongly dependent on the porosity and to a lesser extent on the calcium content. The elastic modulus of jawbone and dentin were compared and the elastic modulus of jawbone was generally higher than that of dentin while the mineral content was lower.

TABLE OF CONTENTS

ABSTRACT	ii
TABLE OF CONTENTS	iv
LIST OF TABLES	viii
LIST OF FIGURES	ix
LIST OF ABBREVIATIONS	xiii
ACKNOWLEDGEMENTS	xiv
CHAPTER 1 INTRODUCTION.....	1
CHAPTER 2 LITERATURE REVIEW.....	3
2.1 Orthopedic and Dental Implants.....	3
2.2 Composition and Structure of Bone and Dentin.....	5
2.3 Techniques for the Characterization of Mineralized Tissues	8
2.3.1 Nanoindentation	9
2.3.1.1 Instrumentations of a Nanoindenter	10
2.3.1.2 Description of the nanoindentation process.....	12
2.3.1.3 Recent studies on the Nanoindentation of Mineralized Tissues.....	14
2.3.2 Quantitative Backscattered Electron Imaging.....	16
2.3.2.1 Recent studies on the qBSEi of Mineralized Tissues	17
2.3.3 Fluorescence Labeling.....	19
CHAPTER 3 RESEARCH SCOPE AND OBJECTIVES.....	21

CHAPTER 4	MATERIALS AND METHODS	23
4.1	Animal Study.....	23
4.1.1	Implant Preparation and Assembly.....	24
4.1.2	Surgery	26
4.1.3	Animal Care after Surgery.....	27
4.1.4	Fluorescence Injections	27
4.1.5	Sample Harvesting.....	27
4.2	Sample Analyses	27
4.2.1	Peri-Implant Bone Analysis	28
4.2.1.1	Peri-Implant Bone Sample Preparations.....	28
4.2.1.2	Fluorescence Microscopy and Indentation Location Selection.....	29
4.2.1.3	Indentation of Peri-Implant Bone	31
4.2.1.4	Statistical Analysis	32
4.2.2	Dentin and Jawbone Analysis.....	32
4.2.2.1	Dentin and Jawbone Sample Preparations.....	32
4.2.2.2	Fluorescence Microscopy and Indentation Location Selection.....	35
4.2.2.3	Indentation of Dentin and Jawbone	38
4.2.2.4	Quantitative Backscattered Electron Imaging	38
4.2.2.4.1	BSE Signal Calibration.....	39
4.2.2.4.2	BSE Signal Standardization	40
4.2.2.4.3	BSE Image and Mineral Content Measurement.....	41
4.2.2.4.4	BSE Image and Volume Fraction Measurement	42
4.2.2.5	Analysis of Drying Time	43

4.2.2.6	Analysis of Florescence Dyes	44
4.2.2.7	Regression and Correlation	45
CHAPTER 5	RESULTS	46
5.1	Elastic Modulus of Peri-Implant Bone	46
5.1.1	Elastic Modulus Comparison of Gap Filling and Pores Filling Bone	46
5.1.2	Elastic Modulus Comparison of Ingrown Bone	49
5.1.3	Elastic Modulus Comparison of Host Bone	50
5.1.4	Elastic Modulus Comparison of Ingrown Bone and Host Bone	52
5.2	Properties of Dentin and Jawbone	55
5.2.1	Analysis of Dentin on the Sagittal Plane	55
5.2.1.1	Elastic Modulus, Mineral Content, and Volume Fraction Distributions of Dentin on the Sagittal Plane	56
5.2.1.2	Correlation between Elastic Modulus, Mineral Content, and Volume Fraction of Dentin in the Sagittal Plane	59
5.2.2	Analysis of Dentin on the Transverse Plane	63
5.2.2.1	Elastic Modulus, Mineral Content, and Volume Fraction Distributions of Dentin in the Transverse Plane	63
5.2.2.2	Correlation between Elastic Modulus, Mineral Content, and Volume Fraction of Dentin in the Transverse Plane	66
5.2.3	Analysis of Jawbone	71
CHAPTER 6	DISCUSSIONS	73
6.1	The Effects of Surface Coatings on the Elastic Modulus of Peri-Implant Bone	73

6.2	Effects of Mineral Content and Porosity on the Elastic Modulus of Dentin.....	75
6.3	Difference between Dentin and Jawbone	81
CHAPTER 7	CONCLUSIONS	82
CHAPTER 8	RECOMMENDATIONS FOR FUTURE WORK.....	83
REFERENCES	84
APPENDIX	91

LIST OF TABLES

Table. 5-1 t-test p values from Ingrown Bone comparison between paired implant types. 50

Table 5-2 t-test p values for comparisons between Ingrown Bone and Host Bone for the different implant types..... 54

LIST OF FIGURES

Figure 2-1 Hierarchical structure of bone (reprint from ref. 28 with permission from Elsevier).....	5
Figure 2-2 A) SEM: human dentin fractured roughly parallel to the pulp cavity surface. B) Schematic illustration of the fibril bundles arranged in a plane perpendicular to the tubule long axis. (Reprint from ref. 27 with permission from Annual Review of Materials Science)	7
Figure 2-3 Illustrated representation of a human premolar and the microstructure of its dentin; A) the sagittal section of the premolar with labels identifying the two parts, crown and root, and its four major tissues, enamel, dentin, cementum, and dental pulp. B) the sagittal section of the dentin; C) the transverse section of the dentin, D) a microscopic view of the dentin tubules (reprint form ref. 31 with permission from Springer)	8
Figure 2-4 Schematic illustration of an instrumented indentation system (Reprinted from ref. 37 with permission from NIST)	10
Figure 2-5 A typical load-displacement plot (Reprinted from ref. 35 with permission from Elsevier).....	12
Figure 2-6 Schematic of a typical load-displacement with CSM loading cycle (Reprinted from ref. 35 with permission from Elsevier)	13
Figure 4-1 Schematic representation of an assembled implant	25
Figure 4-2 X-ray image demonstrating implant location and orientation	26
Figure 4-3 Illustration of a rabbit's distal femur demonstrating observation direction.....	29
Figure 4-4 Fluorescence and white light images of peri-implant bone. 15 days old bone is identified by the calcein green labels on this fluorescence image.....	30

Figure 4-5 Illustration demonstrating bone location classifications. A) Pores Filling Bone; B) Gap Filling Bone; C) Host Bone	31
Figure 4-6 Image of a lower jaw demonstrating directions and planes of interest.....	34
Figure 4-7 Image of a lower jaw (side view) demonstrating directions and plane of interest	35
Figure 4-8 Fluorescence and white light images of a rabbit’s right mandibular incisor (sagittal plane section).....	36
Figure 4-9 Fluorescence and white light images of a rabbit’s bottom left mandibular incisor (transverse plane).....	37
Figure 4-10 Fluorescence and white light images of a rabbit’s jawbone.	38
Figure 4-11 Correlation of BSE greyscale level and Atomic Number.....	40
Figure 4-12 Standardization of BSE signal	41
Figure 4-13 BSE images of dentin and corresponding image for demonstrating grey level discrimination for porosity and dentin. A) transverse plane; B) sagittal plane.	42
Figure 4-14 Elastic modulus of dentin on the sagittal plane at 3 different drying times (3 days, 8 days, and 17 days).	43
Figure 4-15 BSE and corresponding fluorescence images of dentin on the transverse plane.	44
Figure 5-1 Elastic modulus comparison of Gap Filling Bone and Pores Filling Bone. A) from Ta implants; B) from Ta-CaP implants; C) from Ta-CaP-ALN implants. Error bars represent $\pm 1SD$	47
Figure 5-2 Elastic modulus comparison of Ingrown Bone from Ta, Ta-CaP, Ta-CaP-ALN implants. Error bars represent $\pm 1SD$	49

Figure 5-3 Elastic modulus comparison of Host Bone in Ta, Ta-CaP, and Ta-CaP-ALN Implants. Error bars represent $\pm 1SD$.	51
Figure 5-4 Elastic modulus comparison of Ingrown Bone and Host Bone: A) from Ta implants; B) from Ta-CaP implants; C) from Ta-CaP-ALN implants. Error bars represent $\pm 1SD$.	53
Figure 5-5 Elastic modulus distribution of dentin from distal to proximal end on the sagittal plane	57
Figure 5-6 Mineral content distribution of dentin on the sagittal plane	58
Figure 5-7 Volume fraction distribution of intertubular dentin on the sagittal plane	59
Figure 5-8 Scatterplot of elastic modulus vs. mineral content of dentin on the sagittal plane	60
Figure 5-9 Linear regression for the correlation of elastic modulus and mineral content of dentin on the sagittal plane	61
Figure 5-10 Scatterplot of elastic modulus vs. volume fraction of dentin on the sagittal plane	62
Figure 5-11 Linear regression for the correlation of elastic modulus and volume fraction of dentin in the sagittal plane	62
Figure 5-12 Elastic modulus distribution of dentin from anterior growth front to posterior growth front on the transverse plane	64
Figure 5-13 Mineral content distribution of dentin on the transverse plane	65
Figure 5-14 Volume fraction distribution of intertubular dentin on the transverse plane	66
Figure 5-15 Scatterplot of elastic modulus vs. mineral content of dentin in the transverse plane	67

Figure 5-16 Linear regression for the correlation of elastic modulus and mineral content of dentin in the transverse plane	68
Figure 5-17 Scatterplot of elastic modulus vs. volume fraction of dentin on the transverse plane	69
Figure 5-18 Linear regression for the correlation of elastic modulus and volume fraction of dentin in the transverse plane	69
Figure 5-19 Scatterplot of elastic modulus vs. mineral content of jawbone	71
Figure 5-20 Linear regression for the correlation of elastic modulus and mineral content of jawbone.....	72
Figure 6-1 Logarithmic regression for the correlation between elastic modulus and mineral content of dentin in the sagittal plane.....	77
Figure 6-2 Logarithmic regression for the correlation of elastic modulus and volume fraction of dentin in the sagittal plane	78
Figure 6-3 Logarithmic regression for the correlation of elastic modulus and mineral content of dentin on the transverse plane	79
Figure 6-4 Logarithmic regression for the correlation of elastic modulus and volume fraction of dentin on the transverse plane.....	80
Figure 6-5 Elastic modulus vs. mineral content scatter plot of data from jawbone, dentin on the sagittal plane, and dentin on the transverse plane.....	81

LIST OF ABBREVIATIONS

ALN	Alendronate
CaP	Calcium phosphate
ANOVA	Analysis of variance
CSM	Continuous stiffness measurement
VGH	Vancouver General Hospital
ELD	Electrolytic deposition
HA	Hydroxyapatite
PBS	Phosphate buffered saline
PMMA	Poly-(methyl methacrylate)
SD	Standard deviation
SEM	Scanning electron microscope
BSE	Backscattered electron
qBSEi	Quantitative backscattered electron imaging
THR	Total hip replacement
TKR	Total knee replacement
UHMWPE	Ultrahigh molecular weight polyethylene

ACKNOWLEDGEMENTS

I want to thank my supervisor Dr. Rizhi Wang, who not only granted me this excellent opportunity, but also provided me with the inspiration and motivation to complete this research.

I would like to extend my gratitude to Dr. Winston Kim for performing the surgeries, and to Mary Fletcher for her help during the BSE imaging sessions. I would also like to thank Zimmer Inc. and NSERC for their support with the project.

I also want to express appreciation to my colleagues Dr. Ke Duan, YouXin Hu, ShanShan Lu, and Vincent Ebacher, for their friendship and their assistance throughout this research. The time we spent working together in the laboratory was truly delightful. I would like to express my extended gratitude to Dr. Ke Duan for his extensive assistance and support with this research and thesis.

I want to express my deepest thanks and gratuity to the most important people in my life, my friends and my family, for their tremendous love and relentless support. To Matthew Tse, you are the best friend a person can have, and I thank you for your friendship and your support in every aspect of my life. To Beryl Huang, you have given me an infinite amount of love and joy throughout the years, and I am extremely lucky and truly blessed to have you in my life. Thank you my love. To my father, thank you for your love and support. They may not be shown in the most obvious ways, but I can feel them in many ways. To my sister, you have loved and supported me throughout my entire life.

You are a wonderful sibling and an excellent friend to me. Thank you for everything. Finally, to my dearest mother, there is nothing I can say or do to show you my appreciation for your unwavering love, kindness, patience, understanding, and support. I am and will forever be indebted to you. I thank and love you from the bottom of my heart.

Chapter 1 Introduction

Advances in the field of medicine have extended the average human life expectancy worldwide.¹ This means an increasing number of elderly people will suffer from problems associated with their mineralized tissues, and will require orthopedic and dental implants to restore their quality of life.^{2,3,4,5,6,7}

Hip and knee replacements are common orthopedic surgeries performed on the elderly. Between April 1st 2004 and March 31st 2005 there were a total of 58,714 hip and knee replacements performed in Canada. It is projected that the number of surgeries will reach over one hundred thousand in 2014-2015.⁴

In 2005, more than 60% of Canadians have at least one missing tooth.⁸ Dental implants offer a good solution for these people because it prevents jawbone loss, gum recession, and offers better aesthetic and convenience compared with dentures or bridges.⁹ With the expected increase in population, life expectancy and improvements in dental implants, it is anticipated that the market for dental implants will rise in the near future.²

An ideal implant should have mechanical and structural properties compatible with the original mineralized tissue, and should also promote faster and stronger implant fixation.¹⁰ Before such an ideal implant can be designed, the properties of mineralized tissues must be well understood. This thesis focuses on two aspects related to mineralized tissues and implant systems: 1) mechanical properties of peri-implant bone, and 2) mechanical and structural properties of tooth and jawbone.

First, nanoindentation was used to evaluate the elastic modulus of peri-implant bone from a bone-implant animal model. Previous studies have shown that local delivery of alendronate, an anti-osteoporosis drug, enhances new bone formation,^{11,12,13,14,15} but the effects of the drug on the mechanical properties of the new bone is unknown. In this thesis, the elastic moduli of the peri-implant bone with and without the presence of alendronate were compared. Knowledge from this study will improve the understanding of the effect of alendronate on implant fixation, and could expedite the widespread adoption of implants with local anti-osteoporosis drug delivery functions.

Second, nanoindentation and qualitative backscattered electron imaging were used to study the mechanical properties, composition, and structure of dentin and jawbone. A better understanding of dentin and jawbone should help with the improvements of future dental implant designs.¹⁶

Chapter 2 Literature Review

2.1 Orthopedic and Dental Implants

An ideal implant should have mechanical and structural properties compatible with the original mineralized tissue, and should also promote a faster and stronger implant fixation.¹⁰ A fundamental knowledge of orthopedic and dental implants, and the structure and composition of bone and dentin is necessary for the eventual development of such an implant. A brief review on these topics is provided in this and the subsequent section of this chapter.

Hip and knee replacement surgeries are the most common orthopedic implant surgeries performed around the world.¹⁷ The modern total hip replacement (THR) was first introduced by Sir John Charnley of England in the early 1960s, since then many improvements have been made.¹⁸ The majority of THR consists of three major parts, a metallic acetabular cup, a polymer liner, and a metallic femoral head and stem. Currently, most acetabular cups and femoral heads and stems are made of cobalt-chromium alloys or titanium alloys, but porous tantalum acetabular cups are now being manufactured for use.¹¹ The polymer liner is made of ultrahigh molecular weight polyethylene (UHMWPE).¹⁹

The total knee replacement (TKR) was first developed by Dr. Frank Gunston in the late 1960's.^{20,21} The TKR consists of three components, a metallic femoral component, a polymer patellar component, and a metallic tibial component.^{19,22} Similar to the THR, the

metallic components of a TKR are made of cobalt-chromium alloys or titanium alloys, and the polymer patellar component is made of UHMWPE.¹⁹

Modern dental implantology was developed in the mid-1960s by Dr. Per-Ingvar Brånemark, a physician from Gothenburg Sweden.^{21,23} Dental Implants are artificial devices that replace the original root of a tooth, and does not include traditional forms of tooth replacement such as removable prosthetic fixtures (dentures) and other non-root-form implants (crowns and bridges).⁷ Since the early 1980s, the use of dental implants has become a well-established and preferred treatment method to replace missing teeth. Dental implants offer significant advantages over resin-bonded or conventional bridges because they prevent the needless restoration to the adjacent teeth.²⁴

There are several types of dental implants that are in use today. Those types of dental implants include: root form, blade form, Ramus frame and subperiosteal dental. Root form dental implants are the most common dental implants used. There are many variations of root form implants, and each of them have different mounting designs, surface roughness modifications, coatings, or combination of all three to improve implant fixation.²⁵

A root form dental implant looks like a small cylinder or screw and is usually made of titanium. After an implant is placed in the jawbone, a metal collar called an abutment is attached to it. The abutment serves as a base for a crown, denture or bridge.²⁶

2.2 Composition and Structure of Bone and Dentin

Bone is primarily composed of approximately 70 wt% minerals, 25 wt% collagen protein, and 5 wt% water. It has a highly complex structure and can be described as having 7 hierarchical levels of organization.^{27,28} An illustration of the hierarchical structure of bone is presented in Figure 2-1.

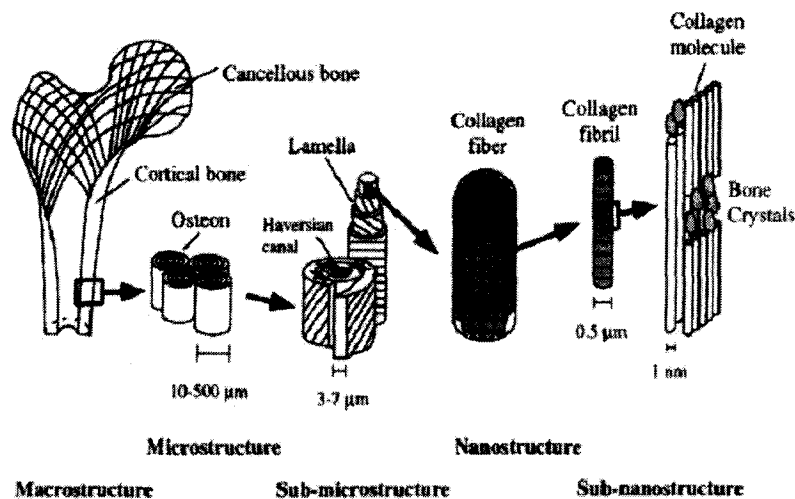


Figure 2-1 Hierarchical structure of bone (reprint from ref. 28 with permission from Elsevier)

At the nanometer scale (level 1 and 2), bone is made up of mineral ($\text{Ca}_{10}(\text{PO}_4)_6(\text{OH})_2$) nanocrystals and collagen fibers that assemble together to form mineralized fibrils. The mineralized collagen fibrils are the building blocks of bone, and are 50-100 nm in diameter and can be up to a few millimeters in length. These mineralized collagen fibrils combine in bundles or arrays and forms mineralized collagen fibers (nanostructure, level 3). Collagen fibers form sheets of lamella, which combine with each other to form a lamellar structure (lamellar bone) at the micrometer scale (level 4).^{27,28}

At the sub-millimeter scale (level 5) osteons, also called Haversian systems, are present in bone. In the center of an osteon there is a channel, called the Haversian canal, which is surrounded by layers of lamellar bone. Haversian canals are created during bone remodeling. During bone remodeling, osteoclast cells resorb bone and create canals. These canals are then refilled by osteoblast cells which rebuild the bone with layers of lamellar bone. The rebuilding process stops when the canals are almost completely filled, and only a narrow channel is left at the center that functions as a blood vessel.^{27,28}

At the macro scale (level 6), bone is classified as either cortical or trabecular.^{27,28} Cortical bone, also known as compact bone, has a porosity range of 5% to 10%. Trabecular bone, also known as cancellous bone or spongy bone, is comparatively less dense and has a porosity of 50% to 90%. Trabecular bone contains more blood vessels and bone cells, and its bulk mechanical properties such as strength and elastic modulus are lower than that of cortical bone. At the 7th level of bone's hierarchical organization, long bones, such as tibias and femurs, are made of a combination of cortical and trabecular bone.²⁸

Dentin is the biggest component of a tooth and is a mineralized tissue that has an overall composition roughly the same as bone. It is composed of approximately 70% minerals, 20% collagen, and 10% water. The dentin structure consists of dentinal tubules a few microns in diameter that are surrounded by mineralized collagen fibrils known as intertubular dentin. At the nanometer scale, intertubular dentin is made up of mineralized collagen fibrils (the building blocks of bone) that are approximately 50 to 100 nm in

diameter and are randomly oriented in a plane roughly perpendicular to the dentinal tubules (See Figure 2-2).^{27,29} Because of the similarity between the composition of bone and dentin, researchers consider dentin to be a type of bone but with a different structure.³⁰

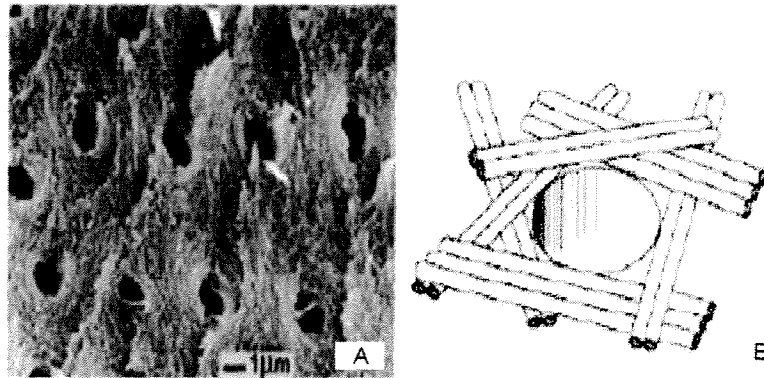


Figure 2-2 A) SEM: human dentin fractured roughly parallel to the pulp cavity surface. B) Schematic illustration of the fibril bundles arranged in a plane perpendicular to the tubule long axis. (Reprint from ref. 27 with permission from Annual Review of Materials Science)

Dentin is filled with nutrient supply routes called dentinal tubules that run from the pulp to the periphery of the tooth (Figure 2-3B).³¹ These dentinal tubules, 1 to 3 microns in diameter, run from the pulp cavity to the periphery with both tubule density and size decreasing toward the periphery (Figure 2-3C).^{29,31} Dentin is formed by odontoblast cells throughout the entire lifetime of the tooth which makes dentin a living tissue.³⁰

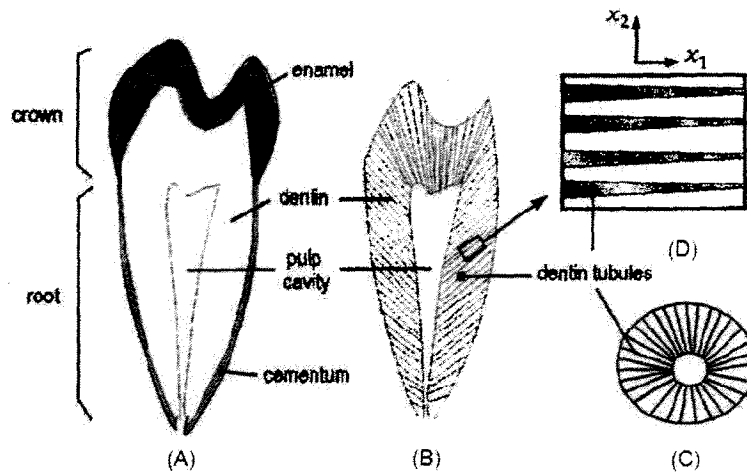


Figure 2-3 Illustrated representation of a human premolar and the microstructure of its dentin; A) the sagittal section of the premolar with labels identifying the two parts, crown and root, and its four major tissues, enamel, dentin, cementum, and dental pulp. B) the sagittal section of the dentin; C) the transverse section of the dentin, D) a microscopic view of the dentin tubules (reprint from ref. 31 with permission from Springer)

2.3 Techniques for the Characterization of Mineralized Tissues

The majority of present day implants require mineralized tissue to grow from a patient's pre-existing host tissues onto/into the surfaces of an implant to create a strong implant fixation.³² This implant fixation has a direct influence on the service life of an implant, which makes the mineralized tissues that create this fixation very important. Poor implant fixation contributes to a high number implant revision surgeries,¹¹ and these surgeries are an additional burden on the already strained Canadian health care system.^{4,6} A better understanding on the properties of mineralized tissues could lead to new implant designs that improve implant fixation and implant compatibility. Properties of mineralized tissues can be investigated with a number of techniques. In this thesis, nanoindentation, quantitative backscattered electron imaging, and fluorescence labeling techniques were used.

Nanoindentation, quantitative backscattered electron imaging, and fluorescence labeling are techniques that have been used extensively to investigate the properties of mineralized tissues; however, they have not been extensively used in combination with each other to study mineralized tissues. A description of these techniques, along with recent studies on mineralized tissues where these techniques are employed, are presented in this and subsequent sections of this chapter.

2.3.1 Nanoindentation

Developed largely over the past three decades, nanoindentation, also known as instrumented indentation testing, or depth-sensing indentation, is a relatively new technique for material testing.³³ Nanoindentation has conventionally been used to study the mechanical properties of metals, ceramics, and polymers, but has since become popular for studying the mechanical properties of mineralized tissues because of its ability to study material at the submicron scale.^{34,35} One of the most often measured properties with nanoindentation is the elastic modulus, a measure of a material's stiffness, or resistance to elastic deformation.^{34,35,36}

2.3.1.1 Instrumentations of a Nanoindenter

A generalized schematic illustration of a nanoindenter is shown in Figure 2-4. All nanoindenter systems have a means for observing and moving the specimen, a means for applying a known force to the indenter shaft, and a means for measuring the resultant displacement.^{34,37} A brief description of the physical mechanisms in a nanoindenter is provided in this section.

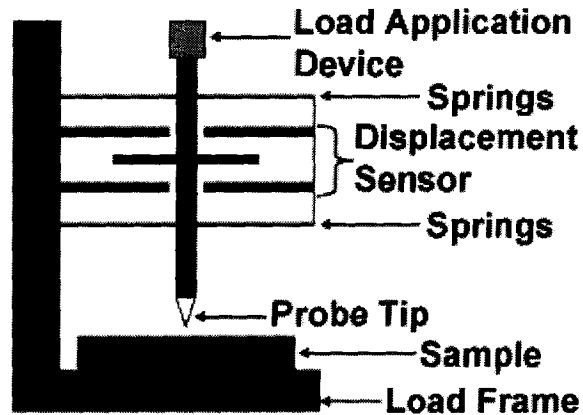


Figure 2-4 Schematic illustration of an instrumented indentation system (Reprinted from ref. 37 with permission from NIST)

The observing and moving of a specimen involves an optical imaging system, and a lateral motion stage. The user initially determines and selects the desired test sites by observing video images through an optical microscope. The magnification of the optical microscope can be 100X, 400X, and 1000X.* After the test sites selection is made, the sample is automatically transported to below the indenter tip by the lateral motion stage, and tests are performed at the selected locations.³⁴

* Specific to Nano Indenter XP

The most popular means for the application of force involves an electromagnetic coil/magnet assembly. This assembly is attached at the top of the indenter shaft and the force imposed, which transfers to the indenter tip, is directly proportional to the current that passes through the coil. The range of load is 0.1 μN to 10 N with a theoretical load resolution of 50 nN.^{*34} It is important to note that the indenter tip, or probe tip, is an important part of a nanoindenter. Usually made of diamond, because of its high hardness and elastic modulus, the Berkovich triangular pyramidal indenter tip is the most common indenter tip used for elastic modulus measurements.^{33,34,37}

A commonly used displacement sensing system involves capacitive sensors consisting of three capacitive plates (circular disks) that can be found around the mid-section of the indenter shaft. The two outside plates are fixed to the stationary head and have an opening that allows the indenter shaft to pass through. The center plate is fixed to the indenter shaft and is free to move vertically between the two stationary plates. The vertical displacement between the stationary and mobile capacitive plates is determined by observing the difference in voltage between them. The range of displacement is 20 nm to 500 μm with a theoretical displacement resolution of less than 0.01 nm.^{*34}

To reduce interferences from the surrounding environment, a nanoindenter system is usually placed on top of a vibration isolation table, and then enclosed by an insulated cabinet.^{34,38}

2.3.1.2 Description of the nanoindentation process

During the course of a nanoindentation process, the indenter tip is pressed into the sample and then withdrawn. During the indenter tip withdrawal, only the elastic portion of the displacement is recovered and this recovery allows the elastic properties of a material to be determined. A record of the depth of penetration and load applied during the entire course of the indentation process (loading and unloading) can be plotted to create a load-displacement curve. Information from the load-displacement curve can be used to calculate the elastic modulus of the sample.^{33,34,37} Figure 2-5 shows a typical load-displacement curve.³⁹

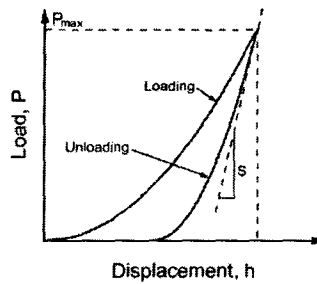


Figure 2-5 A typical load-displacement plot (Reprinted from ref. 35 with permission from Elsevier)

The elastic modulus of the indented sample can be inferred from the initial unloading contact stiffness S , the slope of the initial portion of the unloading curve. From this information, the reduced modulus, E_r , can be calculated by applying

$$E_r = \frac{(\sqrt{\pi} \cdot S)}{2\beta\sqrt{A}} \quad \text{Equation 2-1}$$

where β is a constant that depends on the geometry of the indenter tip, and A is the contact area (for the Berkovich tip $\beta = 1.034$ and $A = 24.56h_c^2$ where h_c is the contact depth).^{33,34,37,39}

E_r , the reduced modulus, accounts for the fact that elastic deformation occurs in both the sample and the indenter. From a sample's E_r , the elastic modulus of a sample can be calculated by

$$\frac{1}{E_r} = \frac{(1-\nu^2)}{E} + \frac{(1-\nu_i^2)}{E_i} \quad \text{Equation 2-2}$$

where E and ν are the elastic modulus and Poisson's ratio for the sample and E_i and ν_i are the elastic modulus and Poisson's ratio for indenter tip. For the diamond Berkovich indenter tip $E_i = 1141$ GPa and $\nu_i = 0.07$.^{33,34,37,39}

The continuous stiffness measurement (CSM) technique is a recently developed technique that offers a significant improvement in nanoindentation testing. The CSM technique allows for the calculation of contact stiffness (S) continuously during loading, instead of only during the unloading portion at the maximum penetration depth. The CSM technique is accomplished by imposing a sufficiently small amplitude harmonic force on top of the primary loading that drives the motion of the indenter (Figure 2-6).^{35,40}

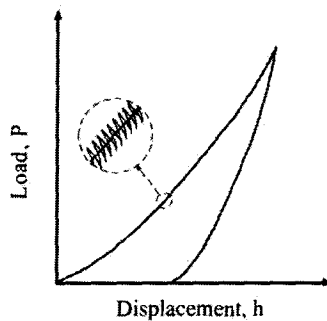


Figure 2-6 Schematic of a typical load-displacement with CSM loading cycle (Reprinted from ref. 35 with permission from Elsevier)

The corresponding displacement oscillation from the harmonic force is monitored and the contact stiffness can be calculated from the phase difference between the force and displacement signals by applying:

$$\tan(\delta) = \frac{\omega D}{S + K_s - m\omega^2} \quad \text{Equation 2-3}$$

where δ is the phase difference between the force and displacement signals, ω is the frequency of the applied force, K_s is the stiffness of the indenter shaft support, and m is the mass of the components.^{35,40,41}

2.3.1.3 Recent studies on the Nanoindentation of Mineralized Tissues

Nanoindentation has been used extensively on studying the elastic modulus of mineralized tissues.^{42,43,44,45} Butz et al. conducted a nanoindentation study on peri-implant bone collected from an animal study. In the animal study, acid-etched and non-acid-etched titanium implants were surgically inserted into the femur of Sprague-Dawley rats. Specimens were removed after 4 weeks of healing time. Butz et al. found that the elastic modulus of peri-implant bone from the etched implants were higher than that from the un-etched sample.⁴⁶

Oyen et al. inserted titanium dental implants into the alveolar ridge of Sinclair miniswines and conducted nanoindentation testing on the jawbone surrounding the implant. After a healing time of 7 months, the implants were harvested and prepared for nanoindentation. The study found that bone closer to the bone-implant interface had lower elastic modulus than bone that was further away.⁴⁷

Saruwatair et al. conducted a nanoindentation study with AFM on mineralized tissues from an in-vitro study with rat bone marrow-derived osteoblast cells. The study found that culturing osteoblast cells on titanium, compared with polystyrene enhanced elastic modulus and interfacial strength of the mineralized tissue. The study also observed that the degree of mineralization of the tissues was higher for titanium than polystyrene and could have been a contributing factor for the increased elastic modulus.⁴⁸

Among the first to apply nanoindentation to the study of dentin was van Meerbeek et al. who measured the elastic modulus of human dentin to be 19.3 GPa. Since then, some researchers have used nanoindentation to determine the elastic modulus of dentin.²⁹ One of the most recent studies was by Kishen et al. Kishen et al. used instrumented microindentation on the sagittal plane of human permanent non-carious lower incisors and an elastic modulus distribution across the plane was established.⁴⁹

Although nanoindentation has been used extensively to study the elastic modulus of mineralized tissues, it has not been widely used for studying peri-implant bone. In addition, studies have not taken into consideration the age of the newly formed mineralized tissues. Additionally, nanoindentation studies on dentin are not as readily available as studies on bone.

2.3.2 Quantitative Backscattered Electron Imaging

Mineral content and porosity are important factors that contribute to the mechanical properties of mineralized tissues.³⁰ Quantitative backscattered electron imaging (qBSEi) is a technique that can be used to quantify the mineral content of mineralized tissues such as dentin, and can also be used to quantify its porosity (volume fraction).^{50,51} One important advantage of qBSEi is that samples previously used for nanoindentation can be reused for imaging. This allows for an effective correlation between data gathered from qBSEi and nanoindentation.

The primary technology behind the qBSEi technique is the Scanning Electron Microscope (SEM).^{38,50,51} To create an image, the SEM focuses a beam of high energy electron (incident electron beam) onto a sample's surface. Different types of signals are generated from the interaction between the incident electron beam and the sample surface, and the signals are detected and processed to create different types of images. One type of signals generated from this interaction is backscattered electrons (BSE) signals.^{38,52}

Originating from the incident electron beam, electrons are reflected or backscattered by the sample. The total number of electrons from the primary beam that are backscattered by the atoms in the sample material determines the intensity of the BSE signal. The number of backscattered electrons is a function of the atomic number of the sample material and the contrast in the BSE image is created by the different intensities recorded. The BSE signal intensity, measured in greylevels (0-255), can be used to quantify the mineral content of mineralized tissues, since regions with a higher average atomic number

(i.e. higher mineral content) appear brighter (lower greyscale levels) than regions of lower atomic number (i.e. lower mineral content). Also, since porosity appears as dark regions on the image, BSE images can also be used to quantify porosity.^{38,53,54,55}

2.3.2.1 Recent studies on the qBSEi of Mineralized Tissues

As previously mentioned, one of the advantages in using the qBSEi technique for mineral content and porosity quantification is that the same samples previously used for nanoindentation can be used for qBSEi.³⁸ Information gathered by qBSEi and nanoindentation can be used to establish correlations between nano-mechanical properties, mineral content, and volume fraction.^{56,57,58,59} This section will present some of the available literatures related to this topic.

Before the mineral content of mineralized tissues can be quantified with BSE images, the BSE signals needs to be calibrated and standardized. Roschger et al. validated a technique for this quantification purpose by using carbon and aluminum as reference materials for backscattered electron signal grey-level calibration, and demineralized bone and hydroxyapatite for calcium concentration standardization.⁵⁷ With this validation technique, this research group conducted studies that correlated elastic modulus with the mineral content in bone.^{60,61} Other publications can be found that correlates elastic modulus with mineral content in bone using nanoindentation and qBSEi; however, publications for this correlation regarding dentin are not as readily available.

Tesch et al. used qBSEi and nanoindentation in an atomic force microscopy and used the calcium content and elastic modulus data collected to conduct a linear correlation analysis. Their study involved BSE imaging and nanoindentation of dentin on the sagittal plane from a human molar, but did not provide a distribution of the properties, and did not consider the age of the dentin.⁵

Angker et al. investigate the use of BSE imaging to quantify the mineral content of sound and carious dentin. Eight primary molars with untreated carious dentin were sagittally sectioned and used for their study. The study found a decrease in calcium content as the distance to pulp decreases.⁵⁶ In another study by the same group, the elastic modulus of carious dentin was measured with indentation, and the calcium content was measured with qBSEi. They found that the deterioration of the elastic modulus of carious dentin was positively correlated to a reduction in its mineral content.⁶²

The elastic modulus of bone is well known to be reduced by porosity and the same is expected for dentin. J. Currey investigated the effects of both calcium content and porosity as explanatory variables on the elastic modulus of bone. In this study, correlations between elastic modulus and both of the explanatory variables were established; however, the study did not provide information on dentin.⁵⁸

Although qBSEi and nanoindentation has been used to study the calcium content and elastic modulus of mineralized tissues, it has not been widely used for dentin. Also,

correlations between the properties of dentin are not vastly available. In addition, past studies have not taken into consideration the age of the mineralized tissues.

2.3.3 Fluorescence Labeling

Fluorochromes, also known as fluorescence labeling, have been used extensively for the histological study mineralized tissues. Fluorochromes are essentially calcium-seeking substances that are incorporated into the mineralization fronts of mineralizing surfaces. After fluorochromes enter the bloodstream, it binds to bone minerals through the chelation of calcium ions at the surface of newly formed apatite crystals. The reason for the selective binding of fluorochromes to newly mineralizing surfaces is unclear; however, it may be associated to the smaller apatite crystal size formed during the initial stages of mineralization.⁶³

Through monitoring the time of fluorochromes administration, the age of newly formed mineralized tissues can be identified. The most commonly used fluorochromes for bone labeling are calcein, alizarin complexone and tetracycline. Newly formed bone with fluorochrome labeling can be identified by the different colors seen when observed under a fluorescent microscope.⁶³

Pautke et al. developed a labeling protocol using multiple fluorochromes. The fluorochromes were sequentially injected into mice during a 4 week period. Bone samples were harvested six months after the final fluorochrome injection. Pautke et al. found that 6 different fluorescent bands could be observed.⁶⁴ With these fluorescent bands, the growth

patterns of bone were observed. In a separate study by the same group, Pautke et al. used similar sequential fluorochrome injections to study the growth of dentin.⁶⁵ Frosch et al. implanted porous titanium into Chinchilla rabbits, and applied 4 different fluorochromes to study the histology of peri-implant ingrown bone. Harvested samples were observed and the peri-implant ingrown bone growth patterns identified.⁶⁶

Although fluorochromes have been used extensively for the histological study of mineralized tissues, this technique has not been used to relate the age of newly formed mineralized tissues with mechanical and structural properties. With the combination of nanoindentation, quantitative backscattered electron imaging and fluorochrome labeling techniques, mechanical and structural information of mineralized tissues can be associated with the exact age of newly formed mineralized tissues.

Chapter 3 Research Scope and Objectives

The scope of this thesis was to investigate the properties of peri-implant bone, dentin, and jawbone using samples harvested from an animal study.

Studies have shown that local delivery of alendronate (an anti-osteoporosis drug) enhances new bone formation; however, the effect the drug has on the elastic modulus of the influenced bone remains unclear. In this thesis, the elastic moduli of the peri-implant bone with and without the presence of alendronate were compared. The peri-implant bone samples were gathered from an animal study. In this thesis, nanoindentation was used to measure the elastic modulus of the peri-implant bone. In addition, fluorochromes were used to identify the age of newly formed mineralized tissues.

There are numerous studies on the composition and mechanical properties of bone. However, studies on the composition and mechanical properties of dentin and the comparison between dentin and bone are not as readily available. In this thesis, dentin and jawbone harvested from an animal study were investigated with nanoindentation and quantitative backscattered electron imaging. Fluorochromes were used to identify the age of newly formed tissues. With the combination of nanoindentation, quantitative backscattered electron imaging and fluorochrome labeling techniques, mechanical and structural information of dentin can be associated with its exact age.

The objectives of this thesis were:

1. To study the effects of surface modifications (calcium phosphate coating and alendronate-immobilized-calcium-phosphate coating) on the elastic modulus of peri-implant bone.
2. To study the elastic modulus, mineral content, and volume fraction distribution of dentin.
3. To establish a correlation between the properties of dentin.
 - a. To establish a correlation between the elastic modulus and mineral content.
 - b. To establish a correlation between the elastic modulus and volume fraction.
 - c. To determine if a correlation between the elastic modulus and both variable (mineral content and volume fraction) is a stronger correlation than those found for objectives 3a and 3b.
4. To compare the elastic modulus and mineral content of dentin and jawbone.

Chapter 4 Materials and Methods

To accomplish the objectives of this research study, a number of methodological steps were taken. The details of the steps involved are presented in this chapter and are organized into two sections, animal study and sample analyses.

The animal study involved implant preparations, surgery, post surgery animal care, fluorescence injections, and sample harvesting. The sample analyses involved sample preparations, nanoindentation, quantitative BSE imaging, and data analysis.

4.1 Animal Study

An animal study was used to accomplish multiple objectives for a number of different research studies and theses. The following section describes the details of the animal study that are relevant to this thesis. For further details regarding this animal study, please refer to reference 11.

Eighteen New Zealand White female rabbits of 3.5-5.0 kg (28 to 34 weeks old) were used in the animal study. They were randomly divided into 3 groups for the surgical implantation of 3 types of implants. The implants were inserted into the distal femurs of the rabbits. Descriptions of the implants and the surgical procedure are provided in subsequent sections of this chapter.

The animal study was conducted at the Jack Bell Centre (animal centre), Vancouver General Hospital. The study was approved by the Animal Research Ethics Review Board at the University of British Columbia (Protocol number: A04-0275).

4.1.1 Implant Preparation and Assembly

Porous tantalum (Trabecular Metal™) cylinders were the main part of the implants used in this study. The porous tantalum cylinders were 3.18 mm in diameter and 8 mm in length. They were manufactured by Zimmer Inc. (Warsaw, Indiana, USA). The specifications, as provided by the manufacture, for the porous tantalum cylinders were as follows: Pore size: 400 to 500 micrometers; Porosity: 75% to 80%; Density of solid tantalum: 16.65 g/cm³; Weight: ≈ 0.237 g.

The porous tantalum cylinders were separated into 3 groups and underwent different surface treatments. The 3 groups were: 1) bare porous tantalum (Ta) group, 2) calcium phosphate coated (Ta-CaP) group, 3) alendronate-immobilized-calcium-phosphate coated (Ta-CaP-ALN) group.

The cylinders in the Ta group were not modified with any surface coatings. The cylinders in the Ta-CaP group were coated with calcium phosphate. The cylinders in the Ta-CaP-ALN group were initially coated with calcium phosphate, then had alendronate immobilized onto it. The calcium phosphate coating and the alendronate immobilization process was developed by Dr. K. Duan, of the UBC Biomaterials research group.¹⁰ The calcium phosphate coating and the subsequent alendronate immobilization for the implants

used in this study were completed by Y.X. Hu, of the UBC Biomaterials research group. The details of the modifications made to the implants can be found in reference number 11.

To better replicate clinical scenarios, a gap model was used. To achieve the effects of a gap during surgery, the porous tantalum cylinders were capped off with polymethylmethacrylate (PMMA) bone cement (Simplex[®] P, Stryker Howmedica Osteonics, Limerick, Ireland) caps at both ends of the cylinders. PMMA bone cement caps were manufactured in house from custom made molds. A drop of bone cement was added into each cap as glue to firmly attach the caps to the ends of the implant cylinder. The assembling of the implants was completed in house. The dimensions of the caps were 4.37 mm in outer diameter, 3.18 mm in inner diameter, 2mm in height and 1.5mm in depth. As a result of these caps, the desired 0.6 mm gap between the porous tantalum cylinder and the surrounding host trabecular bone was maintained after the implants were surgically inserted into the rabbits' femoral bone. After assembly, the implants were placed into the original Zimmer polymer packaging and re-sealed. A schematic representation of an assembled implant is shown in Figure 4-1.

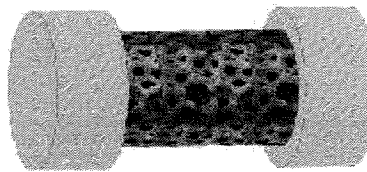


Figure 4-1 Schematic representation of an assembled implant

4.1.2 Surgery

The surgery was performed in an animal operating room inside the Jack Bell Centre by a surgeon, Dr. Winston Kim. Implants were bilaterally inserted (one implant in each femur) into the distal femoral condyle. A 3 cm incision was made with a scalpel at the distal lateral aspect of the femur, and the vastus lateralis was split along its fibers to expose the underlying femoral bone. Through sequential drilling a 4.37 mm opening was made under constant saline irrigation. The orientation of the opening was perpendicular to the distal femoral condyle (Figure 4-2). An implant was inserted into the opening and the wound was then irrigated and closed. The same type of implants was bilaterally inserted into each rabbit to avoid any confounding influences by the presence or absence of different implant coatings. The anesthetic, surgery and animal care were performed in compliance with university and federal guidelines.

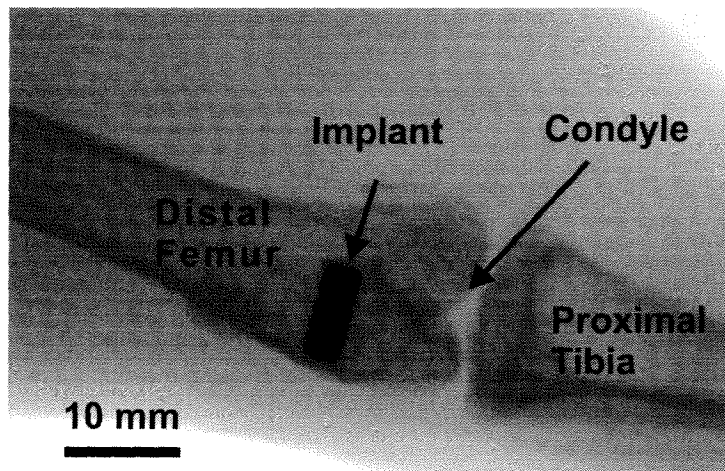


Figure 4-2 X-ray image demonstrating implant location and orientation

4.1.3 Animal Care after Surgery

Antibiotics (Notrile) were administered to the rabbits after the surgeries. The weights and body temperatures of the rabbits were monitored by animal care staff at the Jack Bell Centre.

4.1.4 Fluorescence Injections

Bone and dentin formation fronts were labeled with fluorochromes to track the time of bone/dentin formation. Two commonly used fluorochromes (Sigma-Aldrich, Alizarin) complexone and calcein were used. The labeling chemicals were administered subcutaneously at week 1 and week 2 (calcein, 10mg/Kg), and week 3 and week 4 (alizarin complexone, 30mg/Kg).

4.1.5 Sample Harvesting

The rabbits' distal femurs were harvested 29 days after surgery. After the animals were euthanized, X-ray images of the femur were taken, the lateral legs were dissected, and the femoral bones with the implants were removed. The lower jaw of the rabbits with bare Ta implants were removed and frozen.

4.2 Sample Analyses

The sample analyses for this research are divided into two sections: peri-implant bone, and dentin and jawbone.

4.2.1 Peri-Implant Bone Analysis

4.2.1.1 Peri-Implant Bone Sample Preparations

Prior to the nanoindentation study, the peri-implant bone underwent histology and histomorphometry analysis. This analysis was completed by Y.X. Hu, of the UBC Biomaterials research group.¹¹ Details of the sample preparation relevant to the nanoindentation study are briefly discussed in this section to demonstrate the general history of the samples prior to this study.

The femur was cut parallel to the radius direction of the condyle arc as illustrated in Figure 4-3. The harvested samples were fixed, dehydrated, infiltrated and then embedded in epoxy resin following a standard histological procedure.^{11,67} Each embedded samples were longitudinally cut with a diamond saw (Buehler, Lake Bluff, IL USA), and then ground and polished in the observation direction to 1500 μm from the tangent surface of the implant. After curing, the bottoms of Epothin blocks were ground parallel to sample surface with the grinding fixture at the accuracy of $\pm 20 \mu\text{m}$. The final surfaces were vibration polished with 0.05 micrometer silica slurry. The embedded samples were sputtered with a thin layer of Au/Pd coating and imaged with a Scanning Electron Microscope (Hitachi-S3000N SEM, Hitachi Scientific Instruments, Tokyo, Japan).¹¹

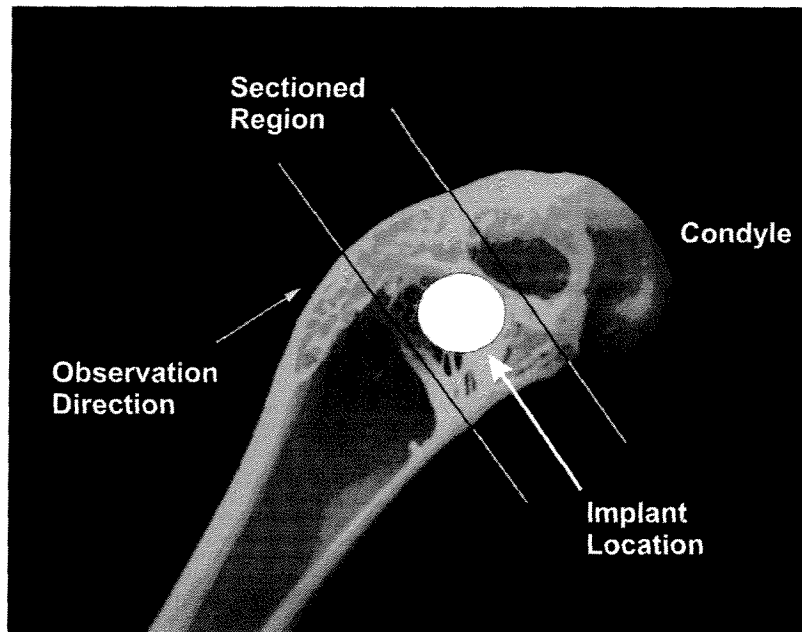


Figure 4-3 Illustration of a rabbit's distal femur demonstrating observation direction

4.2.1.2 Fluorescence Microscopy and Indentation Location Selection

Five samples from each of the 3 groups of implants were randomly selected for the nanoindentation study in this thesis. A fluorescence microscope (Eclipse E 600, Nikon, Tokyo, Japan) with a FITC & TRITC dual exciter and dual emitter filter block, (exciter wavelengths: 475 – 495 nm and 540 – 575 nm, emitter wavelengths 500 – 535 nm and 580 – 620 nm), was used to image the fluorescence labeled peri-implant bone. Under the fluorescence microscope, bone formed on the 7th and 14th day after surgery (22 days old and 15 days old bone) was identified by green calcein labels. Peri-implant bone formed on the 21st and 28th day after surgery (8 days old and 1 day old bone) was identified by the red alizarin labels.

By comparing the fluorescence images with white light images of the same area, the locations for nanoindentations were identified (Figure 4-4). Indentation locations were selected based on the age and physical location of the peri-implant bone.

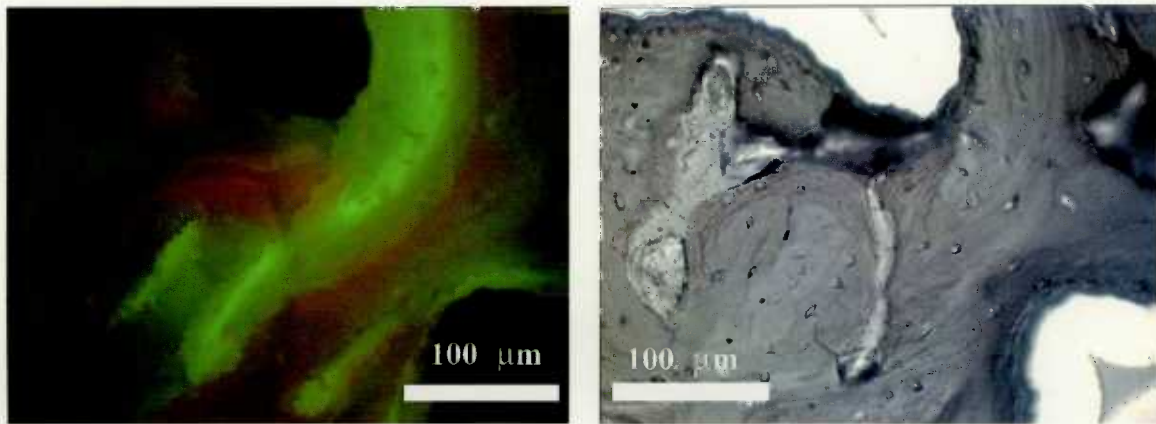


Figure 4-4 Fluorescence and white light images of peri-implant bone. 15 days old bone is identified by the calcein green labels on this fluorescence image.

For this study, the elastic moduli of 15 days old peri-implant bone were measured. The peri-implant bone was classified by its physical location (Figure 4-5). Bone that has grown inside the pores of the porous Ta cylinders was classified as Pores Filling Bone. Bone that has grown into the gap of the implant was classified as Gap Filling Bone. The trabecular host bone surrounding the implant was classified as Host Bone.

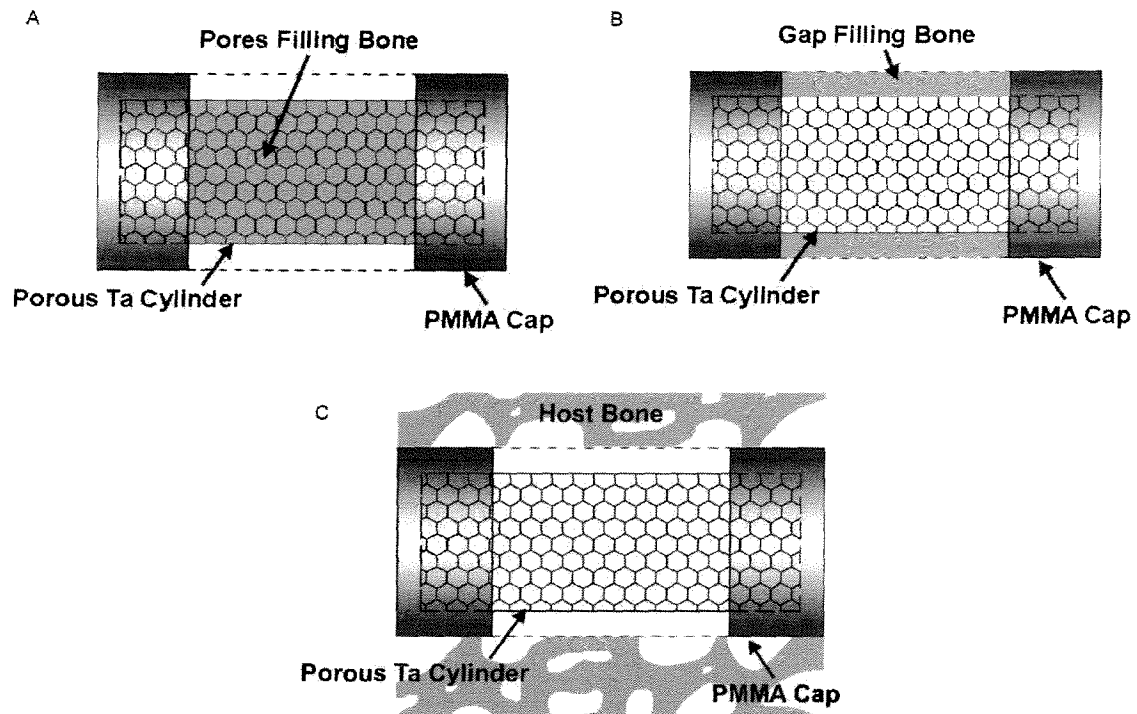


Figure 4-5 Illustration demonstrating bone location classifications. A) Pores Filling Bone; B) Gap Filling Bone; C) Host Bone

4.2.1.3 Indentation of Peri-Implant Bone

A nanoindentation system (Nano Indenter XP System, MTS Nano Instruments, Oak Ridge, TN, USA) was used to measure the elastic modulus of the peri-implant bone. It was measured with a Berkovich diamond tip (AccuTip™) under continuous stiffness measurement mode (CSM). Indenter tip calibration was conducting before indentation testing. The measurements were displacement controlled with penetration depth of 1000 nm. The elastic modulus measured between the depths of 200 and 1000 nm were averaged and used for data analysis. The amplitude and frequency of the sinusoidal signal used were 5 nm and 45 Hz, respectively, the Poisson's ratio was 0.30, and allowable drift rates was set to 0.05 nm/s.^{30,38,68,69,70}

4.2.1.4 Statistical Analysis

Differences in the means and standard deviations of the elastic moduli were characterized with two tailed t-test, ANOVA, and Holm t-test using a statistical analysis software (Primer of Biostatistics, ver. 6.0). The t-test was used to compare the elastic moduli of two groups to identify statistical differences. ANOVA was used to compare the elastic moduli of three groups to identify if statistical differences among the three groups exist and to determine if post hoc analysis was necessary. Holm t-test (post hoc analysis) was used to identify which of the pairs in the three groups were statistically different. A confidence level of 95% was used and a p-value of < 0.05 was considered to be significant.⁷¹

4.2.2 Dentin and Jawbone Analysis

4.2.2.1 Dentin and Jawbone Sample Preparations

Three lower jaws were defrosted and used for this study. The mandibular incisors were removed and submerged into phosphate buffered solution (PBS) for 24 hours before embedding. A standard sample of carbon and aluminum were embedded into each sample block for BSE signal calibration and standardization purposes.

The right mandibular incisors were individually placed lying flat on the medial (flat) surface into standard 1.25 inch diameter molds and embedded with Epothin. After curing, the bottoms of the Epothin blocks were ground parallel to the sample surface with the grinding fixture at an accuracy of ± 20 μm . The sample surface of the Epothin blocks were

then ground to the pulp cavity of the tooth using increasing grits of silicon carbide paper and polished to a mirror finish with 6 and 1 micron diamond suspensions. The final surfaces were vibration polished with 0.05 micrometer silica slurry. These samples were used to investigate the properties of dentin on the sagittal plane (Figure 4-6).

The left mandibular incisors were individually placed in the transverse direction into individual standard molds. The tooth was held in position with a polymer sample holding clip. The tooth was held and embedded in such a way that the crown of the tooth was preserved, and the observation surface was normal to the tangent of the labial (anterior) enamel surface. After curing, the bottoms of the Epothin blocks were ground parallel to the sample surface with the grinding fixture at an accuracy of ± 20 μm . The sample surface of the Epothin blocks were ground to 13 ± 0.5 mm from the crown tip using increasing grits of silicon carbide paper. The sample was then polished to a mirror finish with 6 and 1 micron diamond suspension. The final surfaces were vibration polished with 0.05 micrometer silica slurry. These samples were used to investigate the properties of dentin on the transverse plane (Figure 4-6).

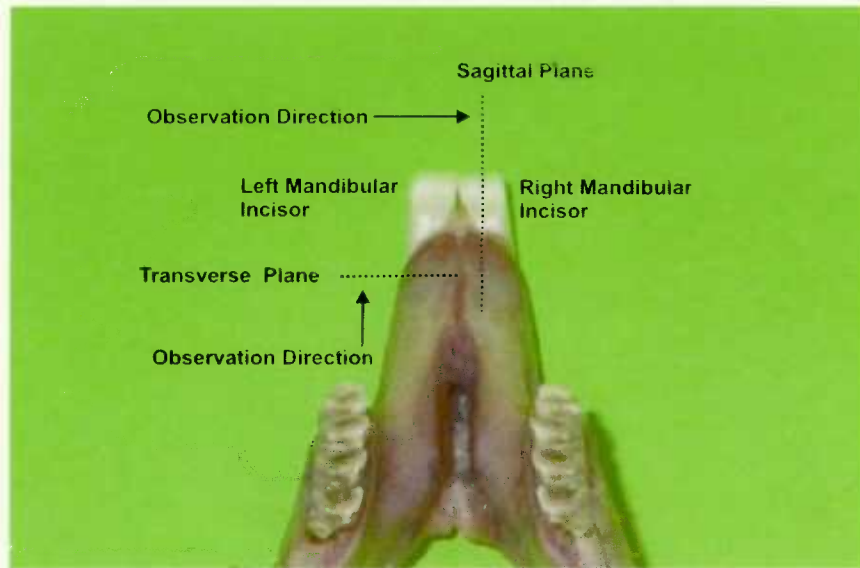


Figure 4-6 Image of a lower jaw demonstrating directions and planes of interest

A section from the left side of the lower jaw was removed. It was cut parallel to the first premolar, exposing the surface of observation (Figure 4-7), and was embedded with Epothin. After curing, the bottoms of the Epothin blocks were ground parallel to the sample surface with the grinding fixture at an accuracy of ± 20 μm . The sample surface of the Epothin blocks were then ground using increasing grits of silicon carbide paper and then polished to a mirror finish with 6 and 1 micron diamond suspension. The final surfaces were vibration polished with 0.05 micrometer silica slurry.

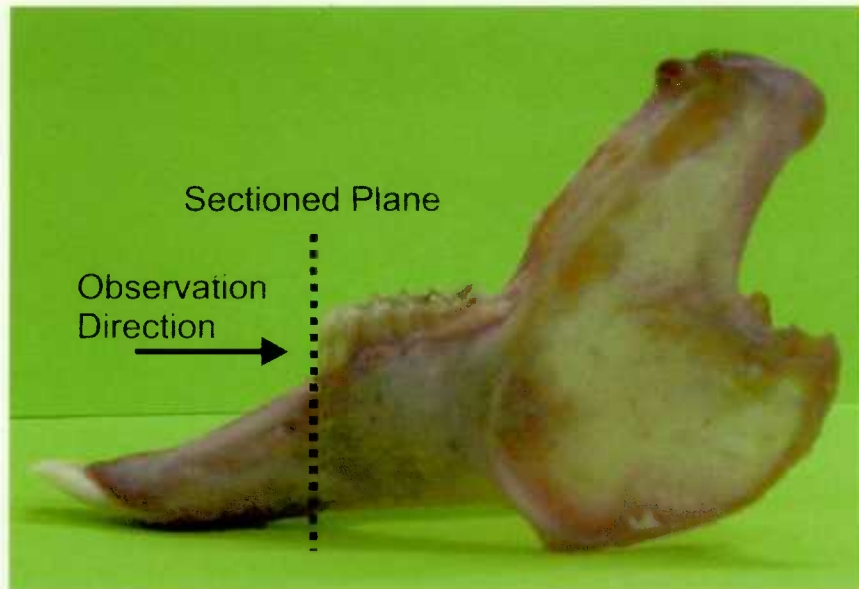


Figure 4-7 Image of a lower jaw (side view) demonstrating directions and plane of interest

Dentin and jawbone sample blocks were then immersed in PBS for 24hr and air dried for 72 hr before nanoindentation.

4.2.2.2 Fluorescence Microscopy and Indentation Location Selection

A fluorescence microscope with a FITC & TRITC dual exciter and dual emitter filter block was used to take images of the fluorescence labeled dentin. Under the fluorescence microscope, dentin formed on the 7th and 14th day after surgery (22 days old and 15 days old dentin) was identified by green calcein labels. Dentin formed on the 21st and 28th day after surgery (8 days old and 1 day old dentin) was identified by the red alizarin label.

By comparing the fluorescence images with white light images of the same area, the locations for nanoindentations were identified. For the investigation of dentin on the sagittal plane, indentations were made on the 22 days old anterior dentin growth front (Figure 4-8).

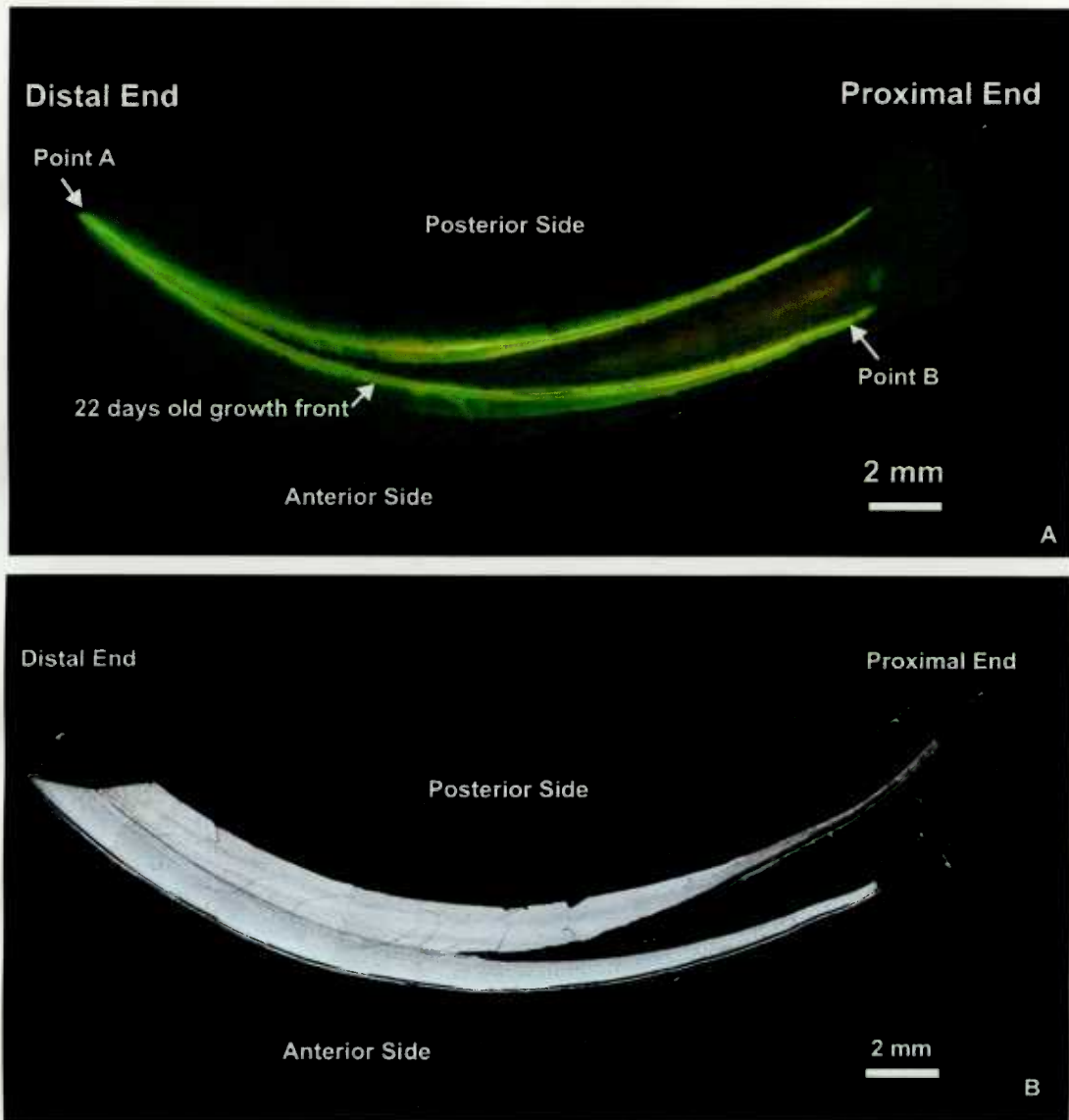


Figure 4-8 Fluorescence and white light images of a rabbit's right mandibular incisor (sagittal plane section)

For the investigation of dentin on the transverse plane, indentations were made on the 22 days old dentin growth fronts (Figure 4-9).

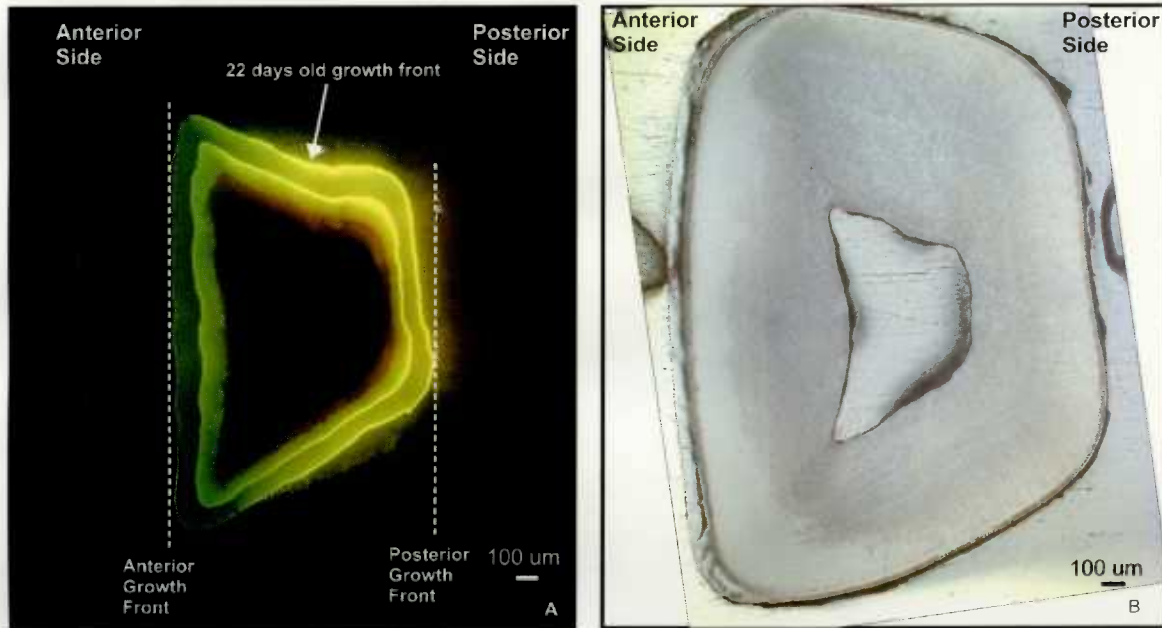


Figure 4-9 Fluorescence and white light images of a rabbit's bottom left mandibular incisor (transverse plane)

For the investigation of jawbone, indentations were made on the 22 days old growth ring in the Haversian systems (Figure 4-10).

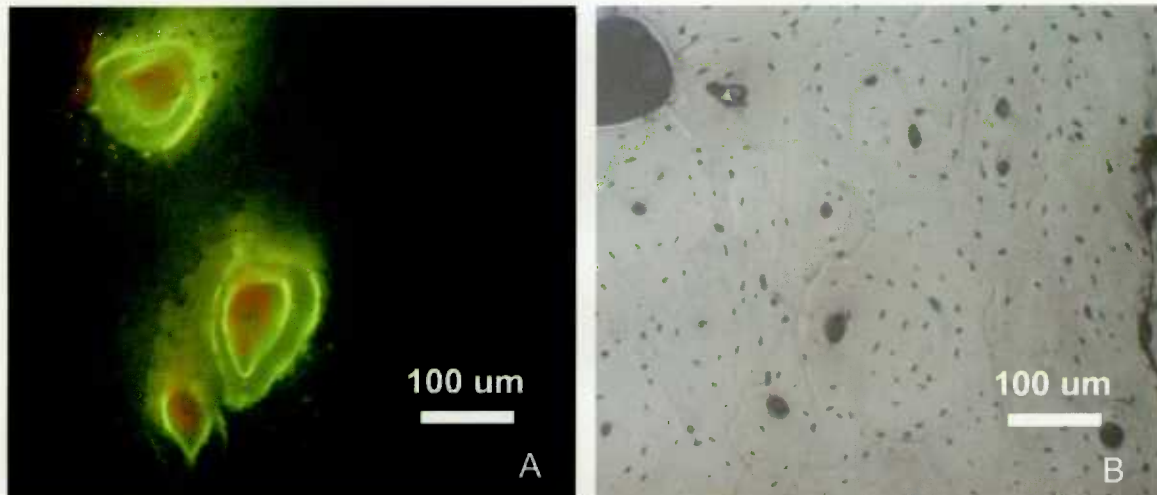


Figure 4-10 Fluorescence and white light images of a rabbit's jawbone.

4.2.2.3 Indentation of Dentin and Jawbone

The Nano Indenter XP System was used to measure the elastic modulus of dentin and jawbone. The elastic modulus was measured with a Berkovich diamond tip under CSM mode. Indenter tip calibration was conducting before indentation testing. The measurements were displacement controlled with penetration depth of 3000 nm. The elastic modulus measured between the depths of 200 and 3000 nm were averaged and used for data analysis. The amplitude and frequency of the sinusoidal signal used were 5 nm and 45 Hz, respectively, the Poisson's ratio was 0.30, and the allowable drift rate was 0.05 nm/s.³⁸

4.2.2.4 Quantitative Backscattered Electron Imaging

Backscattered electron (BSE) imaging was used to quantify the mineral content and porosity of dentin. The samples were carbon coated by vacuum evaporation (JEE-4B

Vacuum Evaporator, JEOL – Japan Electron Optics Laboratory Co. Ltd., Tokyo Japan) to create a conductive surface layer during imaging. BSE images of the indented areas were taken using a scanning electron microscope (Hitachi S-3000N, Hitachi Ltd., Tokyo, Japan). Throughout the BSE imaging process, settings for scanning electron microscope were controlled and monitored. The electron beam energy was set at 20 kV, the working distance was set to 15 mm, magnification of the BSE images was set to 400x, the objective aperture used was 1, the current was monitored, and the contrast and brightness of the images were controlled. BSE images of carbon and aluminum were periodically taken in accordance to changes in the electron beam current. Images were then used for BSE signal standardization.

4.2.2.4.1 BSE Signal Calibration

The calibration of the BSE signals was very important for the mineral quantification of dentin. To determine the atomic number dependence of the BSE signal, two standard materials, carbon (C; $Z = 6$) and aluminum (Al; $Z = 13$), were used. The linearity of the relationship between the atomic number and the BSE greyscale level produced was evaluated with magnesium fluoride (MgF_2 ; $Z = 10.17$), and hydroxyapatite (HA; $Z = 14.43$).⁵⁷ From the results gathered, a calibration curve that provided a correlation between BSE greyscale level (GL) and atomic number (Z) was established. The relationship was a linear function with a R^2 value = 0.9999 (Figure 4-11).

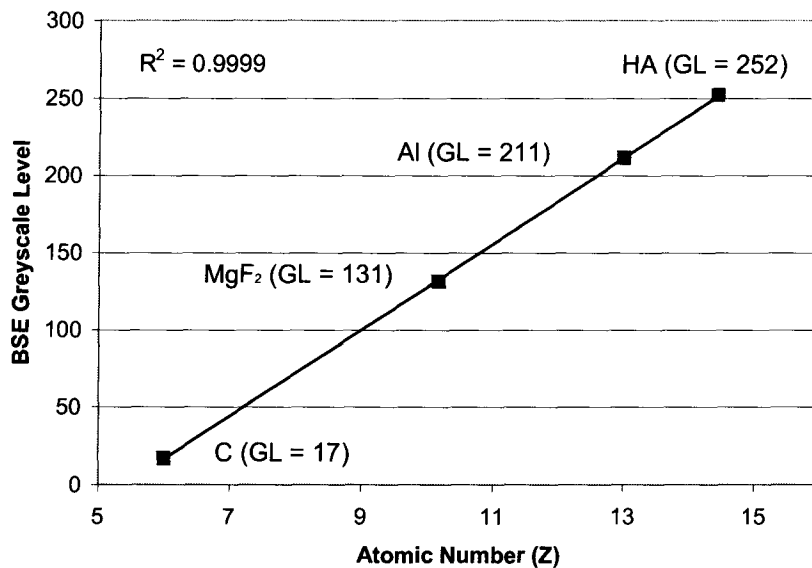


Figure 4-11 Correlation of BSE greyscale level and Atomic Number

The contrast and brightness were adjusted so that the greyscale levels of carbon and aluminum in the BSE images were approximately 20 and 210, respectively. This provides a large greyscale level range suitable for mineral content quantification.

4.2.2.4.2 BSE Signal Standardization

A standardization correlation between BSE greyscale level (GL) and the calcium content (wt% Ca) was necessary for the quantification of mineral content in the dentin samples. A correlation (Figure 4-12) was established by using a standard sample of hydroxyapatite and demineralized bone. The hydroxyapatite (bone mineral) contains 39.86 wt% of calcium in its structure while the demineralized bone (bone matrix) had < 0.2 %. For this correlation, the demineralized bone was considered to have 0 wt% calcium.

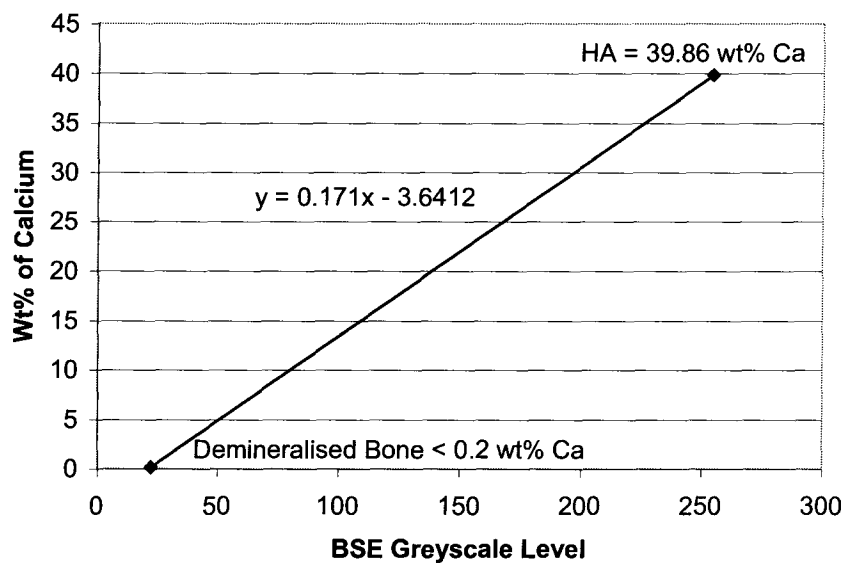


Figure 4-12 Standardization of BSE signal

To complete the standardization correlation between greyscale level and calcium content, a relationship between the demineralized bone sample and carbon greyscale level had to be established. The greyscale level for the demineralized bone sample and carbon were measured under 10 different contrast and brightness settings. The greyscale level of demineralized bone was 5 ± 0.90 greater than that of carbon. This difference was considered during the calcium content measurements.

4.2.2.4.3 BSE Image and Mineral Content Measurement

BSE images were digitally processed using an image analysis/editing software (Corel Photo-Paint X3). Since the nanoindentation imprints were visible on the BSE images, the imprints were digitally removed from the images and the greyscale level of the surrounding dentin were measured and recorded for subsequent calcium content

calculations. Using the greyscale level of periodically taken BSE images of carbon and aluminum, combined with the calibration and standardization methods described in the previous section, the greyscale level measured were converted into weight percentage of calcium (wt% Ca).

4.2.2.4 BSE Image and Volume Fraction Measurement

BSE images were used to measure the volume fraction (V_f) of the intertubular dentin, defined as 100% minus porosity%, of the area surrounding nanoindentation imprints. The BSE images were processed to digitally remove the visible nanoindentation imprints. Using an image analysis software (Clemex Vision Professional Ed. 3.5, Longueuil, QC, Canada), the greyscale level discrimination between porosity and dentin was possible (Figure 4-13). The dentin porosity was measured and converted to the volume fraction.

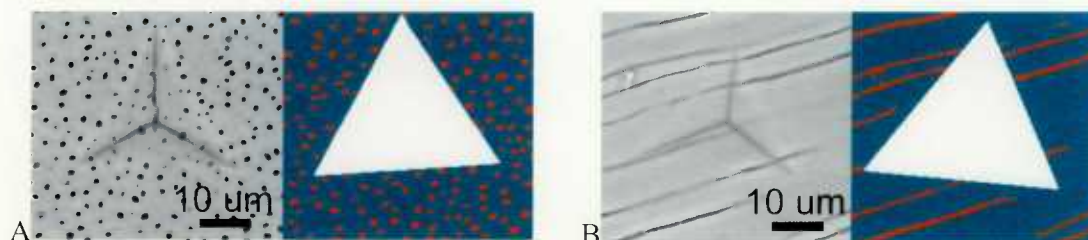


Figure 4-13 BSE images of dentin and corresponding image for demonstrating grey level discrimination for porosity and dentin. A) transverse plane; B) sagittal plane.

4.2.2.5 Analysis of Drying Time

Previous in house studies have found that the elastic modulus of bone remained constant after a drying time of 3 days. Although the same results were expected for dentin, it was necessary to confirm it. Nanoindentations were made on the 22 days old anterior dentin growth front on the sagittal plane after 3 different drying times (3 days, 8 days, and 17 days). Figure 4-14 demonstrates the elastic modulus measurements on the growth front for the three different drying times. It can be observed that the results are similar.

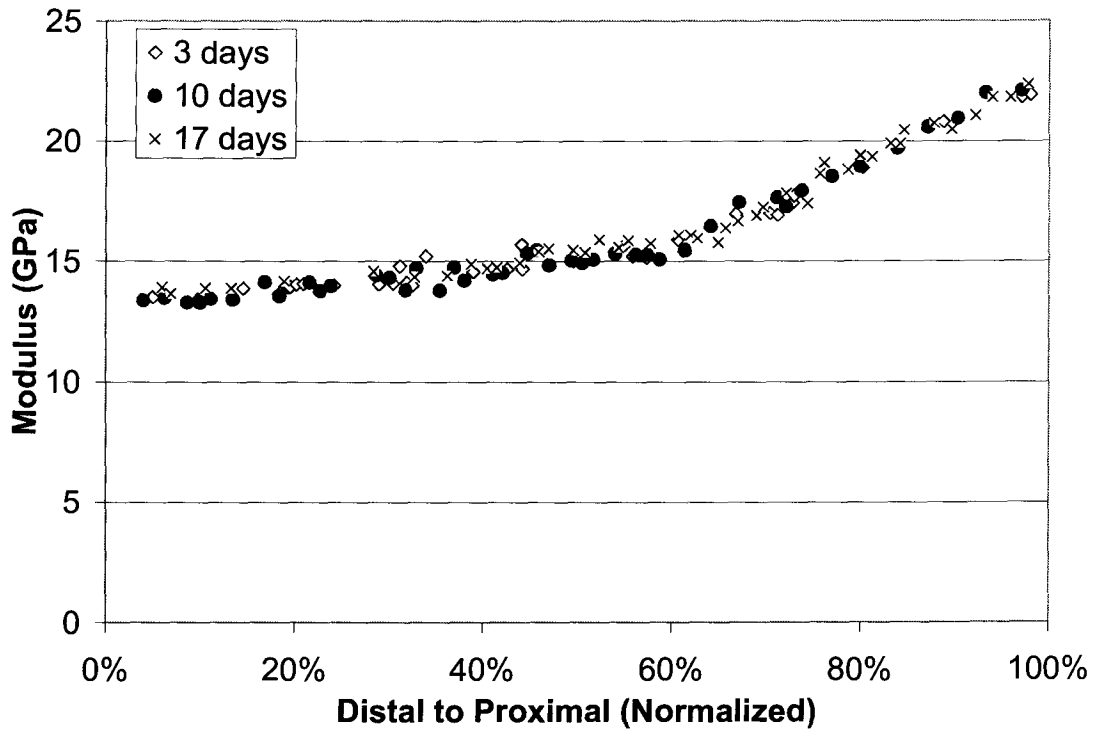


Figure 4-14 Elastic modulus of dentin on the sagittal plane at 3 different drying times (3 days, 8 days, and 17 days).

4.2.2.6 Analysis of Fluorescence Dyes

For this study, it is important to determine if fluorescence dyes, specifically calcein, had an effect on the mineralization of dentin. To determine this, BSE images of dentin on the calcein growth front were analyzed. It can be visually observed that the greyscale level variation throughout the image is minimal (Figure 4-15). Comparing the BSE image with the corresponding fluorescence image from the same area, it can be observed the greyscale level is not affected by the calcein fluorescence.

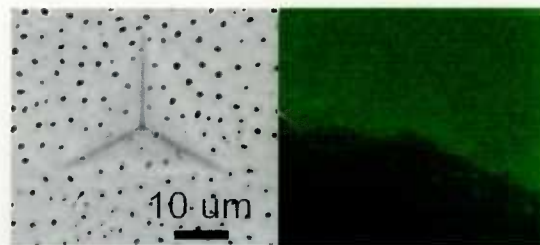


Figure 4-15 BSE and corresponding fluorescence images of dentin on the transverse plane.

To support this observation, ten BSE images were randomly selected and analyzed. The greyscale levels of the areas with and without possible fluorescence influence were measured and compared. The difference in greyscale levels between areas with and without fluorescence was < 3 greyscale level ($< 1\%$). Since the greyscale levels in the BSE images is directly related to the quantified calcium content, if calcein has an effect on mineralization, the effects should be minimal.

4.2.2.7 Regression and Correlation

For this study on dentin, linear regressions were used to determine a correlation between elastic modulus and mineral content (wt% Ca), and elastic modulus and volume fraction (Vf). Afterwards, linear regressions of elastic modulus with both variables (wt% Ca and Vf) were used to establish a correlation coefficient (R). These linear regressions were used for dentin on both the sagittal plane and the transverse plane. A linear regression was also used to establish a correlation between elastic modulus and mineral content in jawbone. In addition to the linear regressions, logarithmic regressions were also used. The regression and correlation results are presented in subsequent chapters of this thesis.

Chapter 5 Results

5.1 Elastic Modulus of Peri-Implant Bone

Porous tantalum implants with different surface modifications were implanted into New Zealand White Rabbits during an animal study. The implants were harvested and the elastic modulus of the peri-implant bone was measured using nanoindentation. To eliminate the effects age may have on the elastic modulus of bone, the age of bone tested was 15 days old. Differences between the elastic moduli of different categories of bone were compared with two tailed t-test, ANOVA, and Holm t-test. A confidence level of 95% was used and a p-value of < 0.05 was considered to be significant. At least 20 nanoindentation measurements were made per bone category per sample. The results from the nanoindentation testing are presented in this section.

5.1.1 Elastic Modulus Comparison of Gap Filling and Pores Filling Bone

A gap implant model was used to better represent a clinical scenario. As a result of this gap, the bone-implant interface was formed by bone that has grown into two distinct regions of the implant, the gap and the pores. The elastic modulus of Gap Filling Bone and Pores Filling Bone are compared in Figure 5-1. Individual comparisons were made for each of the implant types.

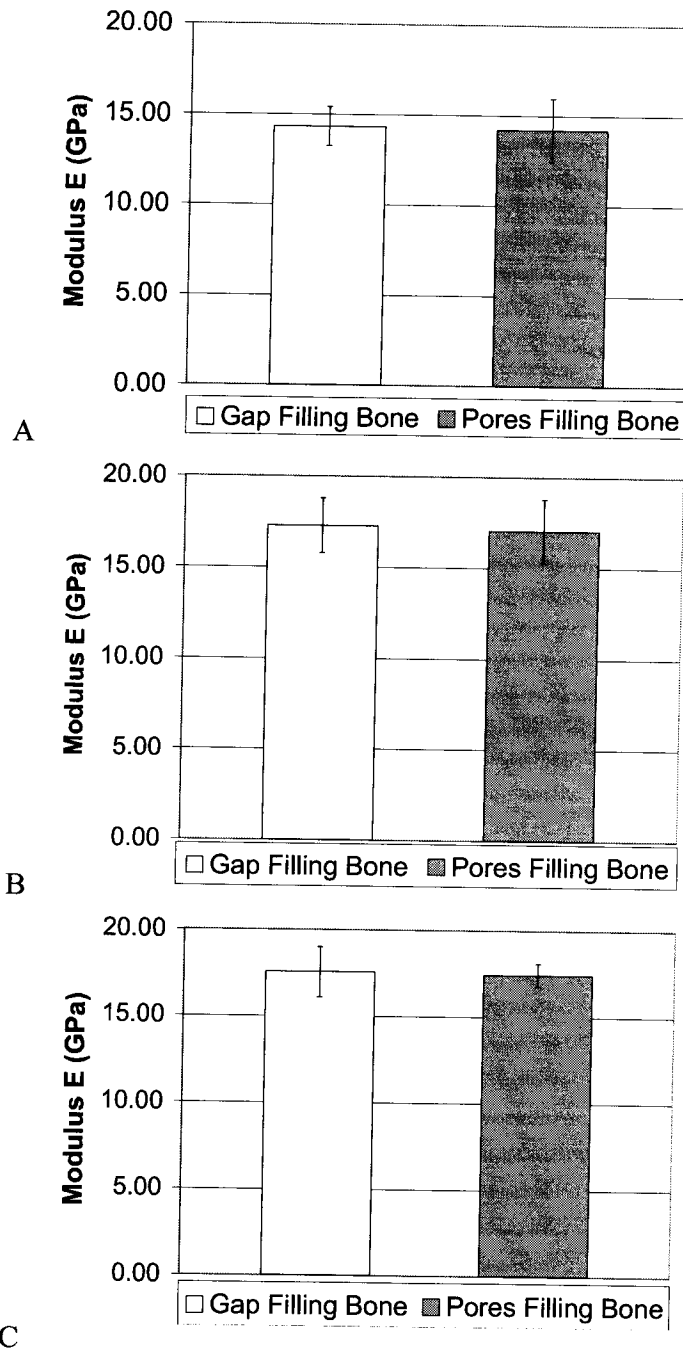


Figure 5-1 Elastic modulus comparison of Gap Filling Bone and Pores Filling Bone. A) from Ta implants; B) from Ta-CaP implants; C) from Ta-CaP-ALN implants. Error bars represent $\pm 1SD$.

The elastic moduli of Gap Filling Bone and Pores Filling Bone from Ta implants were 14.39 ± 1.07 GPa and 14.18 ± 1.75 GPa, respectively. The elastic moduli of Gap Filling Bone and Pores Filling Bone from Ta-CaP implants were 17.25 ± 1.50 GPa and 17.05 ± 1.75 GPa, respectively. The elastic moduli of Gap Filling Bone and Pores Filling Bone from Ta-CaP-ALN implants were 17.52 ± 1.47 GPa and 17.42 ± 0.66 GPa, respectively.

The implant type with the largest elastic modulus difference between Gap Filling Bone and Pores Filling Bone was the Ta group; however, even though the difference was the largest, the difference was less than 0.21 GPa and statistically insignificant (P value > 0.82). Therefore, to reduce complexities, the data for Gap Filling Bone and Pores Filling Bone were combined and re-categorized as Ingrown Bone.

5.1.2 Elastic Modulus Comparison of Ingrown Bone

The elastic moduli of Ingrown Bone from all three implant types are compared in Figure 5.2.

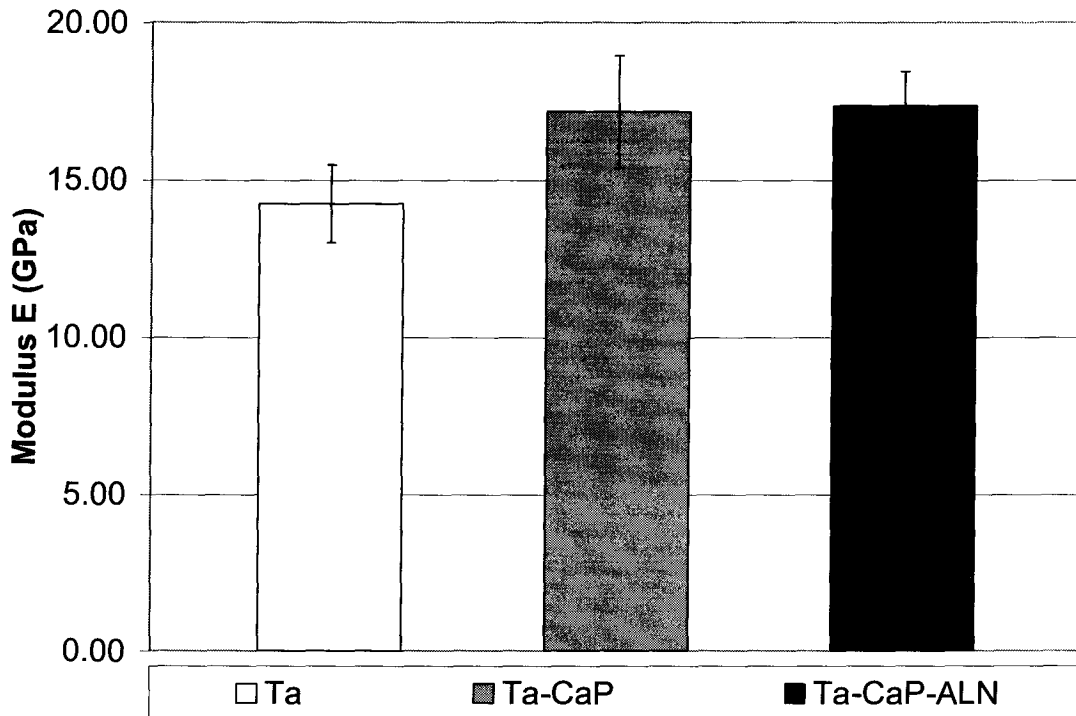


Figure 5-2 Elastic modulus comparison of Ingrown Bone from Ta, Ta-CaP, Ta-CaP-ALN implants. Error bars represent $\pm 1SD$.

The elastic moduli of Ingrown Bone harvested from the Ta, Ta-CaP, and Ta-CaP-ALN implants were 14.24 ± 1.23 GPa, 17.17 ± 1.79 GPa and 17.40 ± 1.10 GPa, respectively. ANOVA statistical comparisons found the elastic modulus differences of Ingrown Bone amongst the three groups to be significant (P value of 0.007). To determine which of the groups are statically different from each other, post hoc analysis for multiple comparison testing is required. Table. 5-1 shows p values from t-tests between implant groups.

Table. 5-1 t-test p values from Ingrown Bone comparison between paired implant types.

Compared Groups	p values
Ta & Ta-CaP	0.019
Ta & Ta-CaP-ALN	0.003
Ta-CaP & Ta-CaP-ALN	0.85

Using a critical p value of 0.05 and applying the Holm t-test shows that the elastic modulus differences between the Ta and Ta-CaP group, and Ta and Ta-CaP-ALN are both statistically significant. The elastic modulus difference between Ta-CaP and Ta-CaP-ALN was statistically insignificant.

The results suggests that the calcium phosphate coatings, with or without alendronate, increased the elastic modulus of the 15 days old Ingrown Bone. The results also suggests that the presence of alendronate did not significantly increase the elastic modulus of the 15 days old Ingrown Bone.

5.1.3 Elastic Modulus Comparison of Host Bone

To determine whether the effects of the surface modifications were limited to the Ingrown Bone, a comparison between the Host Bone from the 3 implant types was conducted and presented in Figure 5-3.

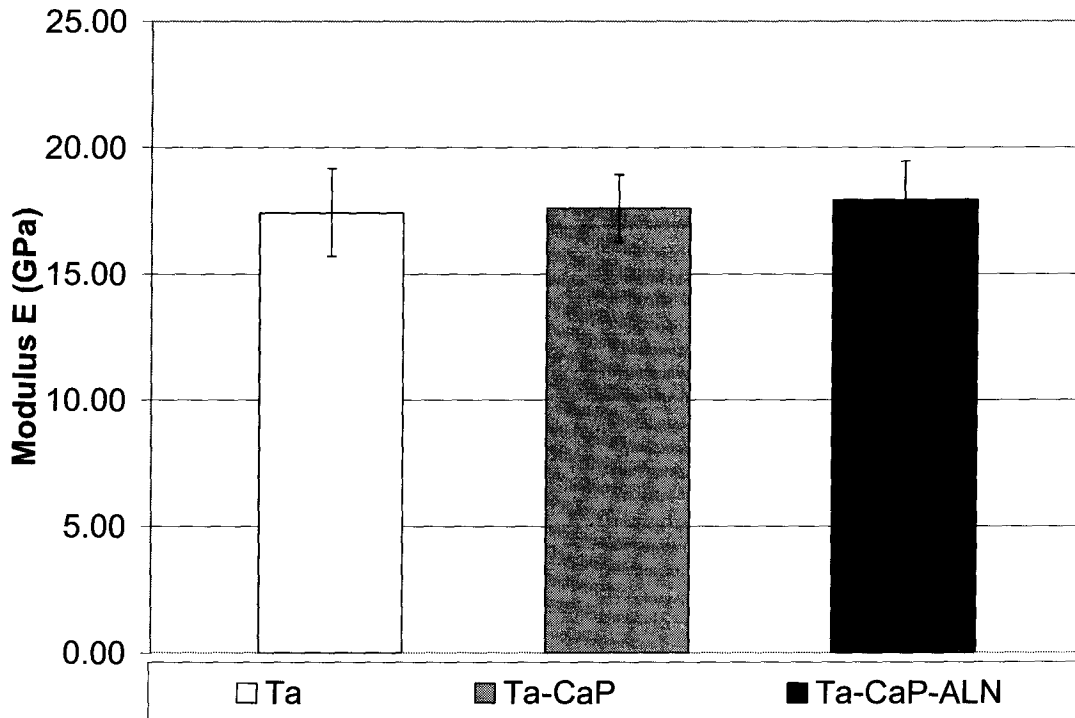


Figure 5-3 Elastic modulus comparison of Host Bone in Ta, Ta-CaP, and Ta-CaP-ALN Implants. Error bars represent $\pm 1SD$.

The elastic modulus of Host Bone from the Ta, Ta-CaP, and Ta-CaP-ALN implants are 17.41 ± 1.74 GPa, 17.59 ± 1.33 GPa, and 17.93 ± 1.52 GPa, respectively. ANOVA statistical comparison found the differences amongst the three groups to be insignificant (P value of 0.865); therefore, post hoc analysis was not required.

The results suggests that the calcium phosphate coatings, with or without alendronate, did not significantly affect the elastic modulus of the Host Bone.

5.1.4 Elastic Modulus Comparison of Ingrown Bone and Host Bone

To determine the differences between Ingrown Bone and Host Bone, the elastic moduli of Ingrown Bone and Host bone are compared in Figure 5-4. Individual comparisons were made for each of the implant types.

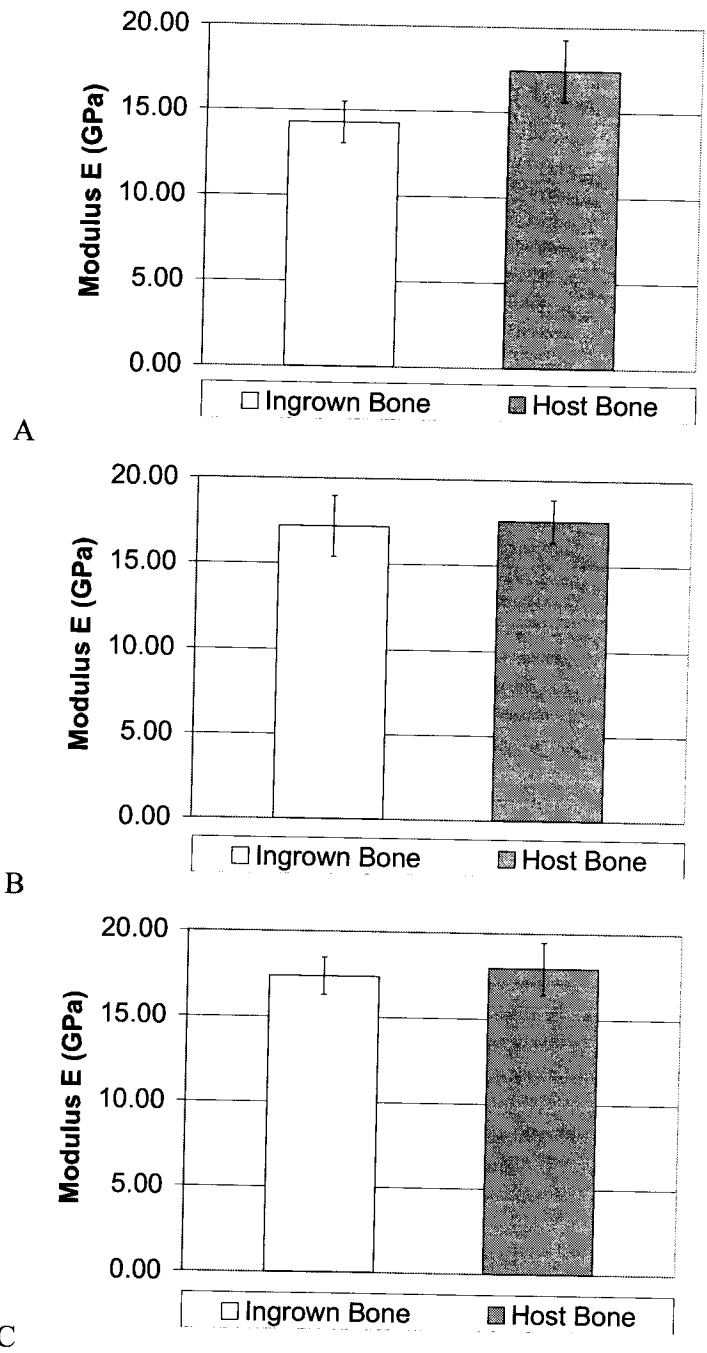


Figure 5-4 Elastic modulus comparison of Ingrown Bone and Host Bone: A) from Ta implants; B) from Ta-CaP implants; C) from Ta-CaP-ALN implants. Error bars represent \pm 1SD.

The elastic moduli of Ingrown Bone and Host Bone from Ta implants were 14.24 ± 1.23 GPa and 17.41 ± 1.74 GPa, respectively. The elastic moduli of Ingrown Bone and Host Bone from Ta-CaP implants were 17.17 ± 1.79 GPa and 17.59 ± 1.33 GPa, respectively. The elastic moduli of Ingrown Bone and Host Bone from Ta-CaP-ALN implants were 17.40 ± 1.10 GPa and 17.93 ± 1.52 GPa, respectively. The elastic modulus differences between the Ingrown Bone and Host Bone for Ta, Ta-CaP, and Ta-CaP-ALN are 3.17 GPa, 0.42 GPa, and 0.57 GPa, respectively.

Table 5-2 t-test p values for comparisons between Ingrown Bone and Host Bone for the different implant types.

Implant Type	p values
Ta	0.012
Ta-CaP	0.685
Ta-CaP-ALN	0.514

Using a critical p value of 0.05, the results indicate that the difference between Ingrown Bone and Host Bone in the Ta samples were statistically significant. On the other hand, there is no statistical difference between Ingrown Bone and Host Bone in the Ta-CaP and Ta-CaP-ALN samples.

The results suggests that the calcium phosphate coatings, with or without alendronate, increased the elastic modulus of the 15 days old Ingrown Bone to that of their respective Host Bone.

5.2 Properties of Dentin and Jawbone

Dentin and jawbone samples were harvested from an animal test. The dentin samples used were from the incisors of the animals' lower jaw. The dentin samples were investigated on two planes, the sagittal plane and the transverse plane. To eliminate the effects age may have on the properties of dentin, the age of the tested dentin was of 22 days old. The elastic modulus of the dentin was measured with nanoindentation, and the mineral content and porosity (volume fraction) of the intertubular dentin were measured from BSE images. The results from nanoindentation and BSE image analyses are presented in this section. Linear regression and correlation of elastic modulus, mineral content, and volume fraction are also presented in this section. The numbers (60, 61, 62) in the legends of Figure 5-5 to Figure 5-19 identifies the rabbit which the mineralized samples were taken from. Each number represents individual rabbits.

The elastic modulus of jawbone was measured using nanoindentation. The age of the tested bone was 22 days old. The results from the nanoindentation and BSE image analyses are presented in this section. Linear regression and correlation between the elastic modulus and mineral content are also presented in this section.

5.2.1 Analysis of Dentin on the Sagittal Plane

The elastic modulus, mineral content, and volume fraction distributions across the length of the dentin on the 22 days old anterior growth front on the sagittal plane are

presented in this section. Correlations between elastic modulus, mineral content, and volume fraction of dentin in the sagittal plane are also presented.

5.2.1.1 Elastic Modulus, Mineral Content, and Volume Fraction

Distributions of Dentin on the Sagittal Plane

For the purpose of demonstrating the distribution of elastic modulus, mineral content, and volume fraction, the length of the teeth were normalized by using the point where the growth front meets the pulp at the distal (crown) end of the tooth (point A in Figure 4-8) as the starting point (0%), and where the growth front meets the dentin enamel junction at the proximal (root) end of the tooth (point B in Figure 4-8) as the ending point (100%). This was required because of the slight variations in lengths between the different tooth samples. The distance between 22 days old dentin and the pulp cavity was not sufficient for nanoindentations in the initial $\approx 5\%$ length; therefore, data for the elastic modulus, mineral content and volume fraction was not available prior to that length.

The elastic modulus distribution from the distal end towards the proximal end of dentin is presented in Figure 5-5.

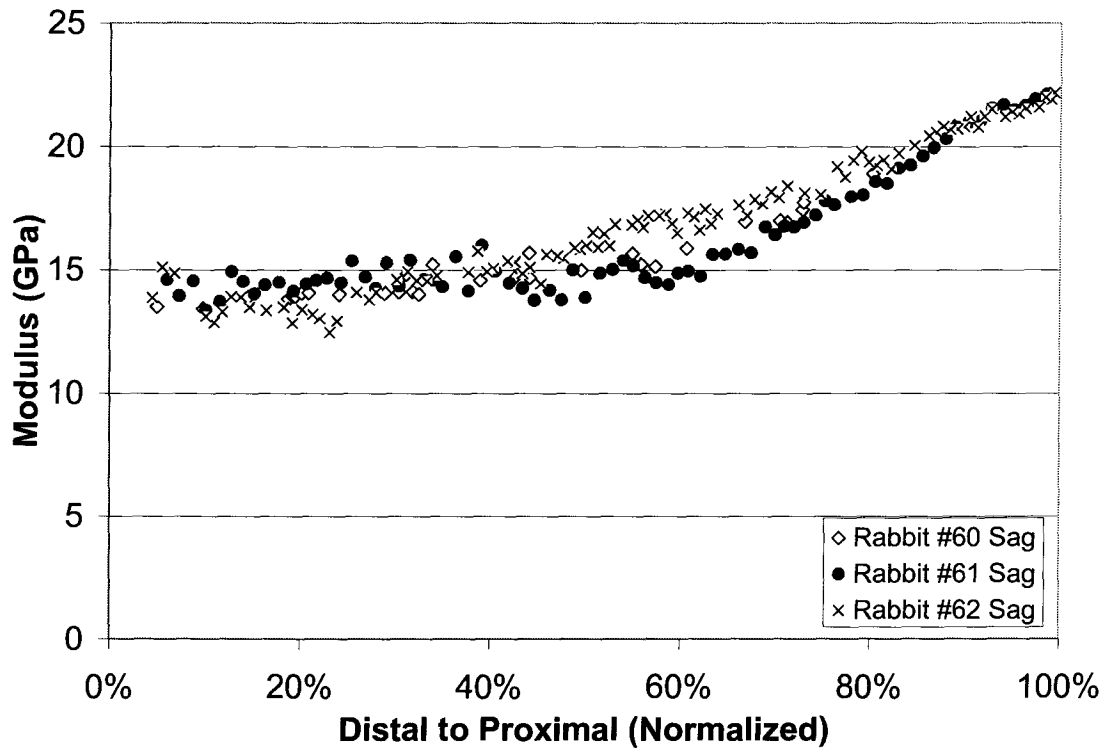


Figure 5-5 Elastic modulus distribution of dentin from distal to proximal end on the sagittal plane

The elastic modulus of dentin on the sagittal plane varies between approximately 12 GPa and 22 GPa. In general, the elastic modulus increases from the crown towards the root of the tooth. The rate of increase for the elastic modulus dramatically increased at approximately 50% to 60% of the length.

BSE images were used to quantify the mineral content (wt% Ca) of dentin on the sagittal plane. The mineral content distribution from the distal end towards the proximal end of the tooth is presented in Figure 5-6.

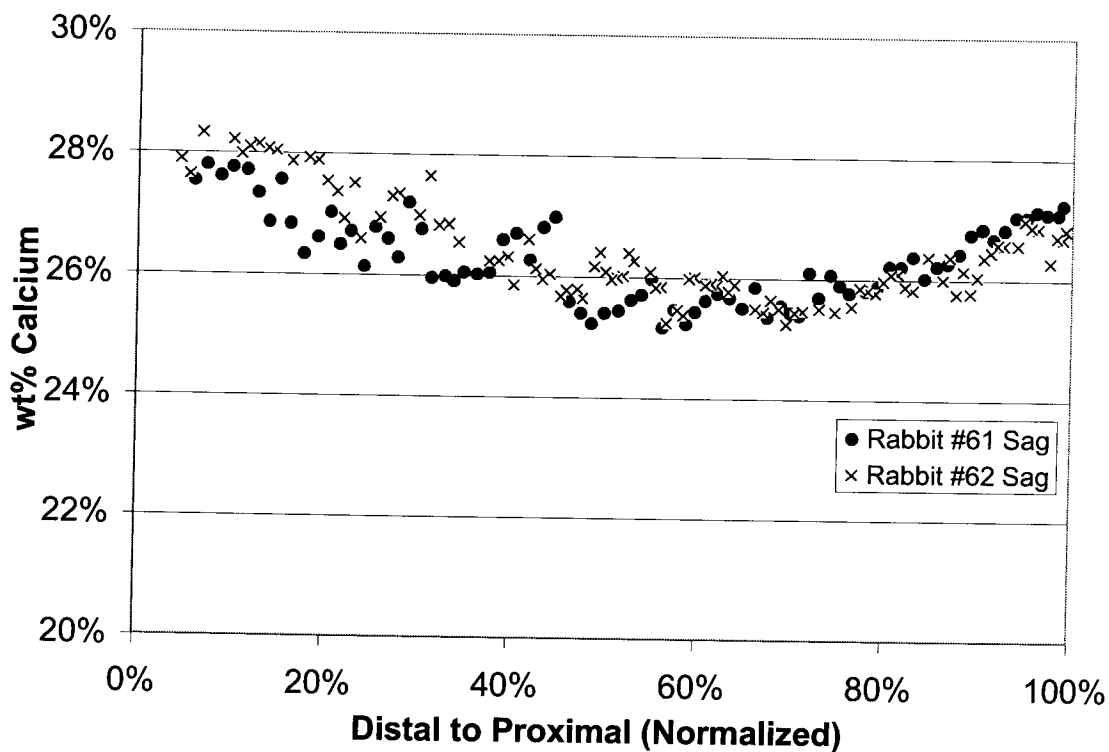


Figure 5-6 Mineral content distribution of dentin on the sagittal plane

The mineral content of dentin on the sagittal plane varies between approximately 25 Wt% Ca and 28 Wt% Ca. In general, the mineral content is lower at the midsection of the tooth.

BSE images were also used to quantify the volume fraction of intertubular dentin on the sagittal plane. The volume fraction distribution from the distal end towards the proximal end of the tooth is presented in Figure 5-7.

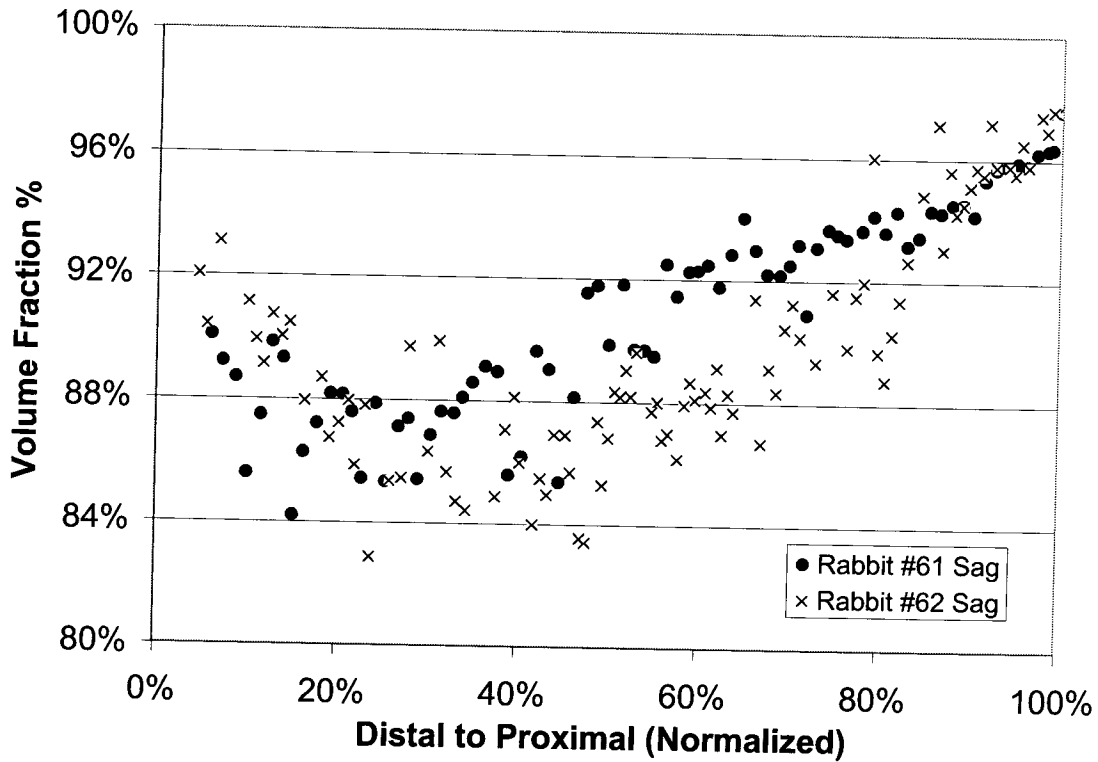


Figure 5-7 Volume fraction distribution of intertubular dentin on the sagittal plane

The volume fraction of intertubular dentin on the sagittal plane varies between approximately 83% and 98%. In general, the volume fraction is lowest at 20% to 30% of the length. It can also be noted that the volume fraction is highest at the root of the tooth.

5.2.1.2 Correlation between Elastic Modulus, Mineral Content, and Volume Fraction of Dentin in the Sagittal Plane

A scatterplot of elastic modulus versus mineral content for dentin on the sagittal plane is presented in Figure 5-8. A linear regression for the correlation of elastic modulus and mineral content is presented in Figure 5-9.

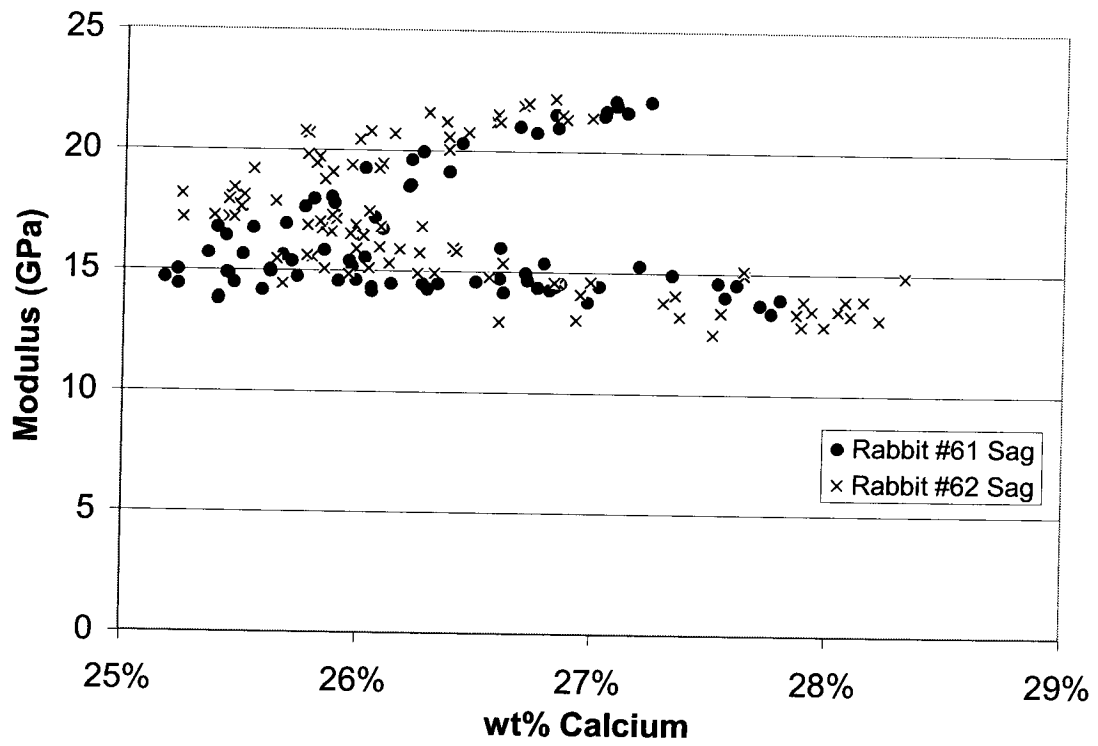


Figure 5-8 Scatterplot of elastic modulus vs. mineral content of dentin on the sagittal plane

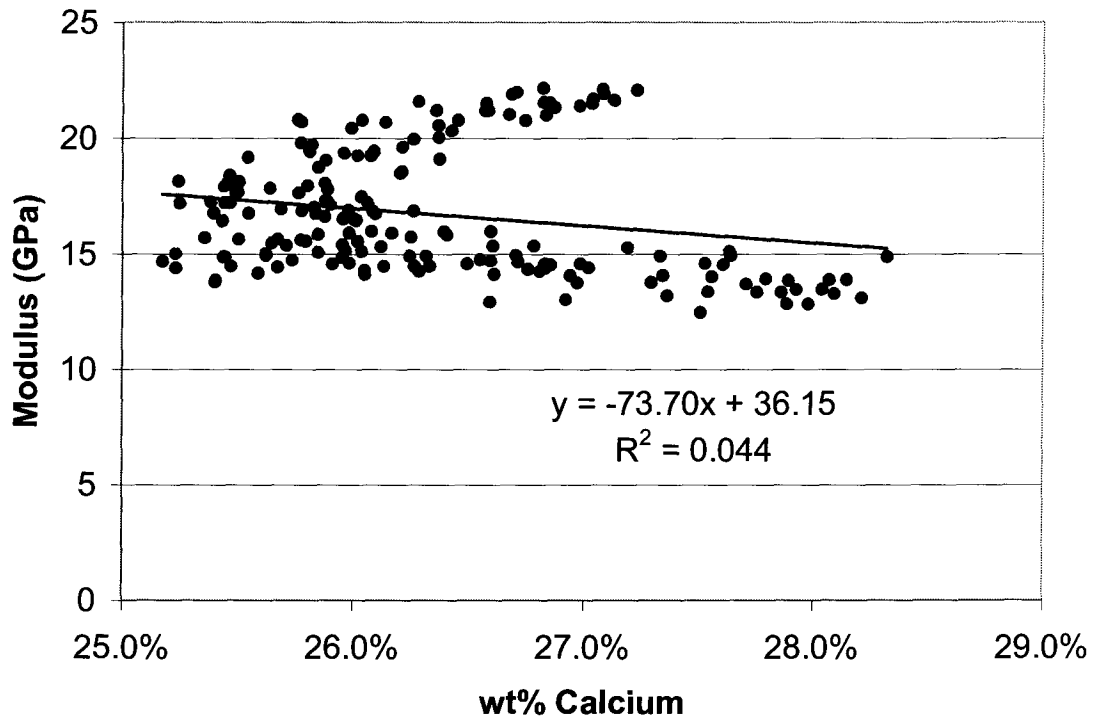


Figure 5-9 Linear regression for the correlation of elastic modulus and mineral content of dentin on the sagittal plane

The correlation coefficient (R) for the regression of elastic modulus and mineral content for dentin on the sagittal plane is 0.21 with a p value of < 0.001.

A scatterplot of elastic modulus versus volume fraction for dentin on the sagittal plane is presented Figure 5-10. A linear regression for the correlation of elastic modulus and volume fraction is presented in Figure 5-11.

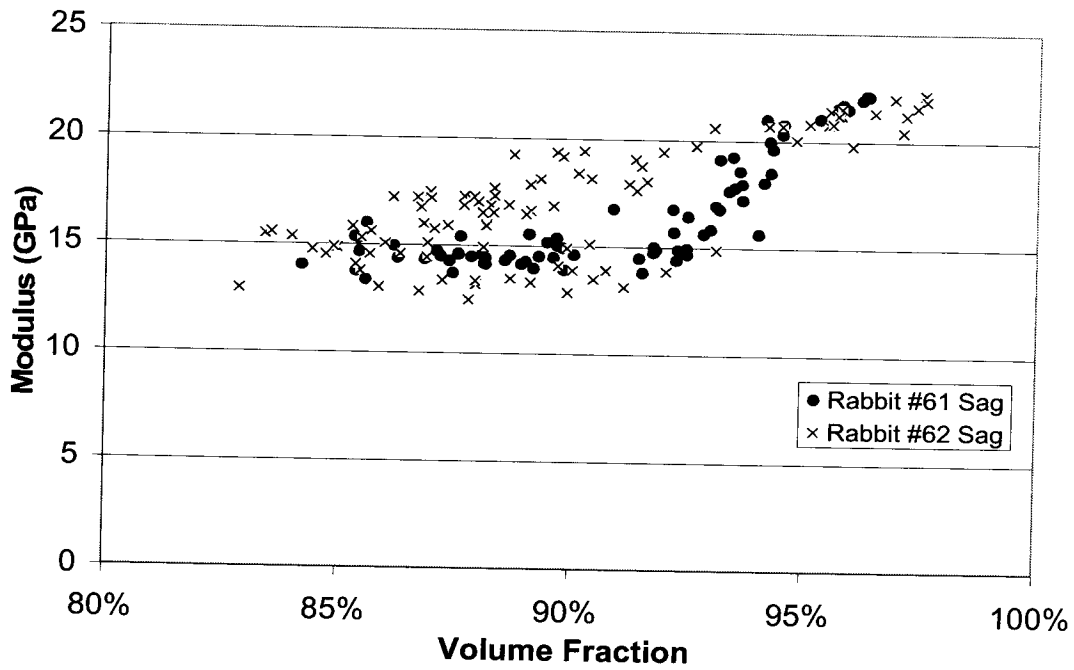


Figure 5-10 Scatterplot of elastic modulus vs. volume fraction of dentin on the sagittal plane

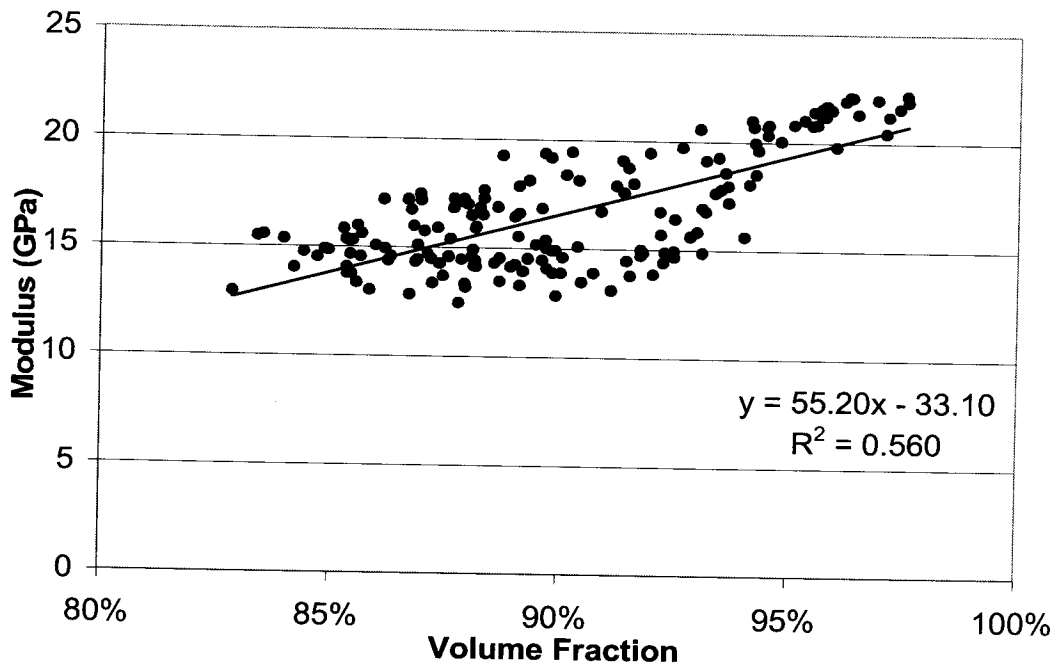


Figure 5-11 Linear regression for the correlation of elastic modulus and volume fraction of dentin in the sagittal plane

The correlation coefficient for the regression of elastic modulus and volume fraction for dentin in the sagittal plane is 0.75 with a p value of < 0.001.

To determine whether or not both mineral content and volume fraction are explanatory variables that have independent effects on the elastic modulus of dentin in the sagittal plane, a multiple linear regression was conducted using both variables. The correlation coefficient for this multiple linear regression was 0.77 ($R^2 = 0.590$) with a p value of < 0.001.

5.2.2 Analysis of Dentin on the Transverse Plane

The elastic modulus, mineral content, and volume fraction distributions of dentin on the transverse plane are presented in this section. Correlations between elastic modulus, mineral content, and volume fraction of dentin in the transverse plane are also presented in this section.

5.2.2.1 Elastic Modulus, Mineral Content, and Volume Fraction

Distributions of Dentin in the Transverse Plane

For the purpose of demonstrating the distribution of elastic modulus, mineral content, and volume fraction, the widths of the teeth were normalized by using the distance between the anterior growth front as 0% distance, and the posterior growth front as 100%

distance (Figure 4-9). This was required because of the slight variations in widths between the different tooth samples.

The elastic modulus of dentin on the transverse plane was measured. The elastic modulus distribution from the anterior growth front towards the posterior growth front is presented in Figure 5-12.

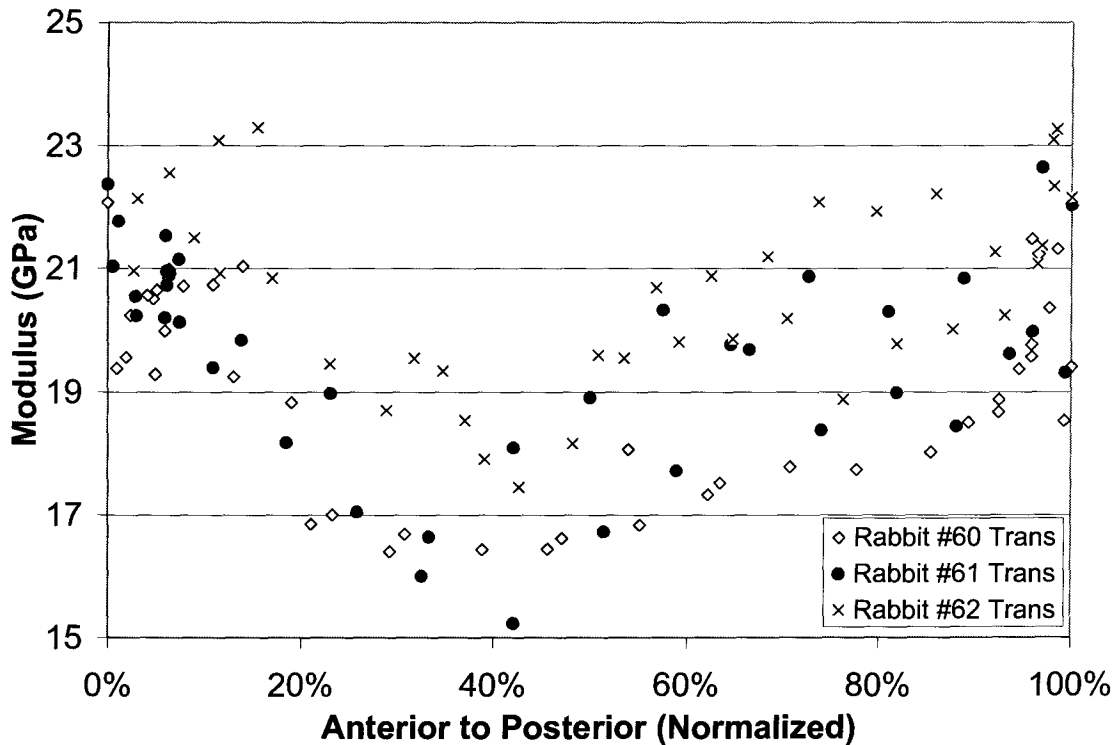


Figure 5-12 Elastic modulus distribution of dentin from anterior growth front to posterior growth front on the transverse plane

The elastic modulus of dentin on the transverse plane varies between approximately 15.5 GPa and 23.5 GPa. In general, the elastic modulus is the lowest between approximately 40% and 50% distance from the anterior growth front.

BSE images were used to quantify the mineral content of dentin on the transverse plane. The mineral content distribution from the anterior growth front towards the posterior growth front is presented in Figure 5-13.

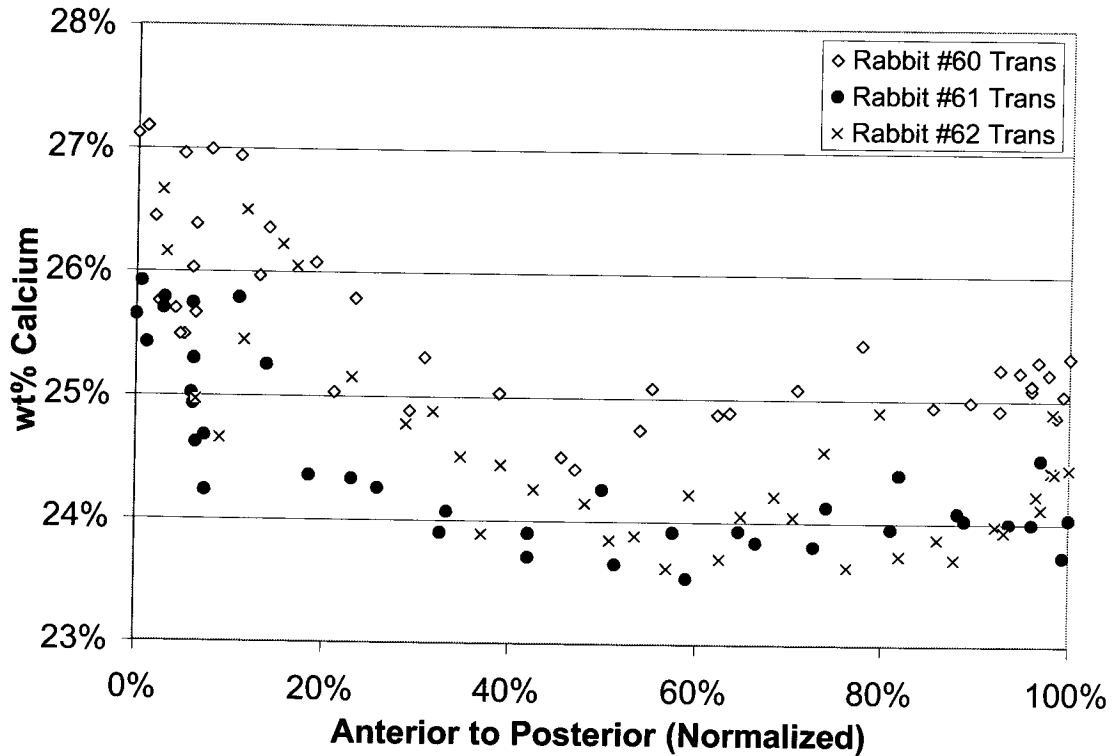


Figure 5-13 Mineral content distribution of dentin on the transverse plane

The mineral content of dentin on the transverse plane varies between approximately 24 Wt% Ca and 27.5 Wt% Ca. In general, the mineral content is lowest between approximately 40% and 60% distance from the anterior growth front.

BSE images were also used to quantify the volume fraction of intertubular dentin on the transverse plane. The volume fraction distribution from the anterior growth front towards the posterior growth front is presented in Figure 5-14.

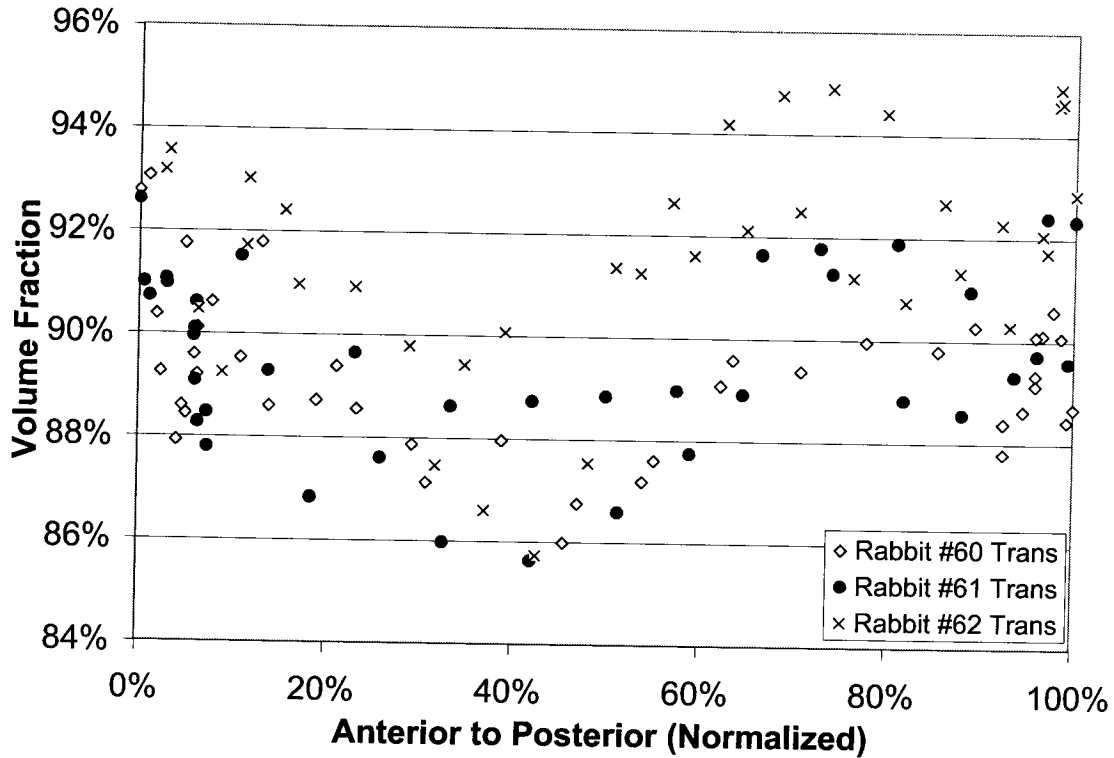
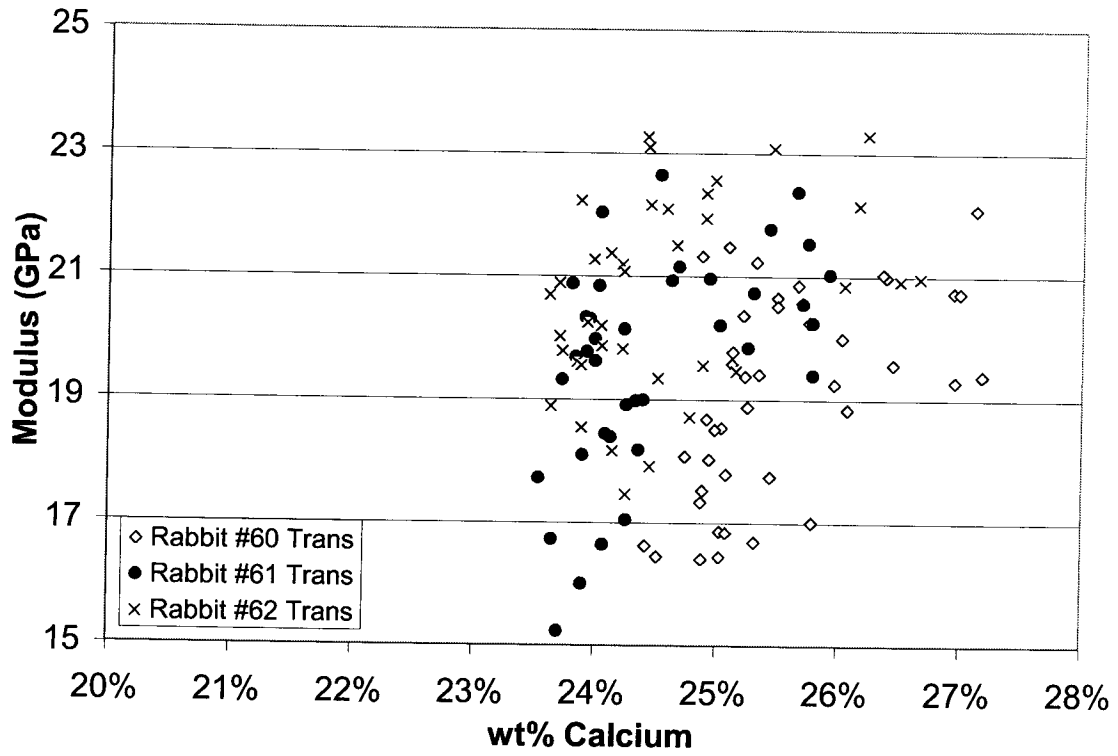


Figure 5-14 Volume fraction distribution of intertubular dentin on the transverse plane

The volume fraction of intertubular dentin on the transverse plane varies between approximately 86% and 95%. In general, the elastic modulus is lowest between approximately 30% and 40% distance from the anterior growth front.

5.2.2.2 Correlation between Elastic Modulus, Mineral Content, and Volume Fraction of Dentin in the Transverse Plane

A scatterplot of elastic modulus versus mineral content for dentin in the transverse plane is presented in Figure 5-15. A linear regression for the correlation of elastic modulus and mineral content is presented in Figure 5-16.



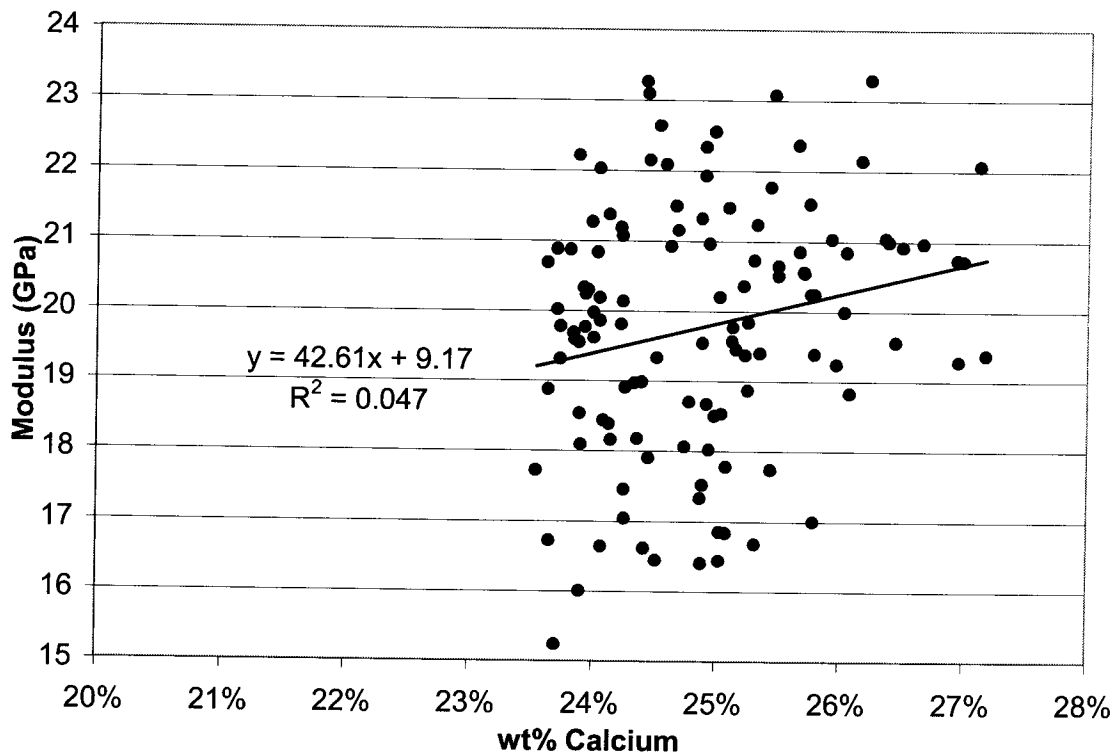


Figure 5-16 Linear regression for the correlation of elastic modulus and mineral content of dentin in the transverse plane

The correlation coefficient for the regression of elastic modulus on mineral content for dentin on the transverse plane is 0.22 with a p value of < 0.001.

A scatterplot of elastic modulus versus volume fraction for dentin in the transverse plane is presented in Figure 5-17. A linear regression for the correlation of elastic modulus and volume fraction was calculated and presented in Figure 5-18.

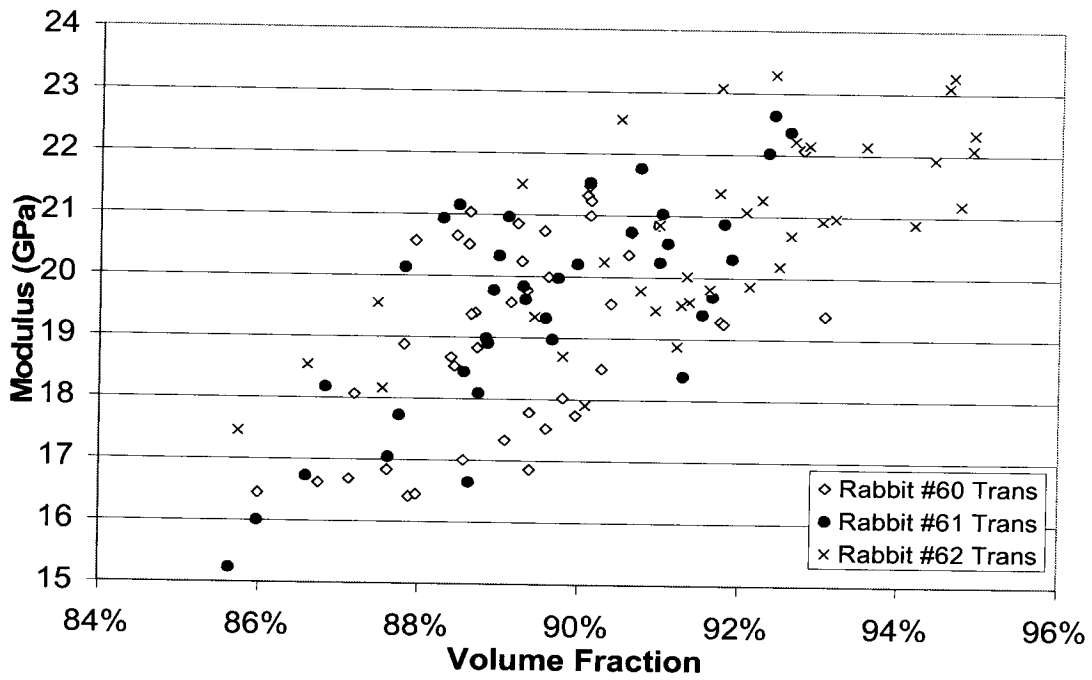


Figure 5-17 Scatterplot of elastic modulus vs. volume fraction of dentin on the transverse plane

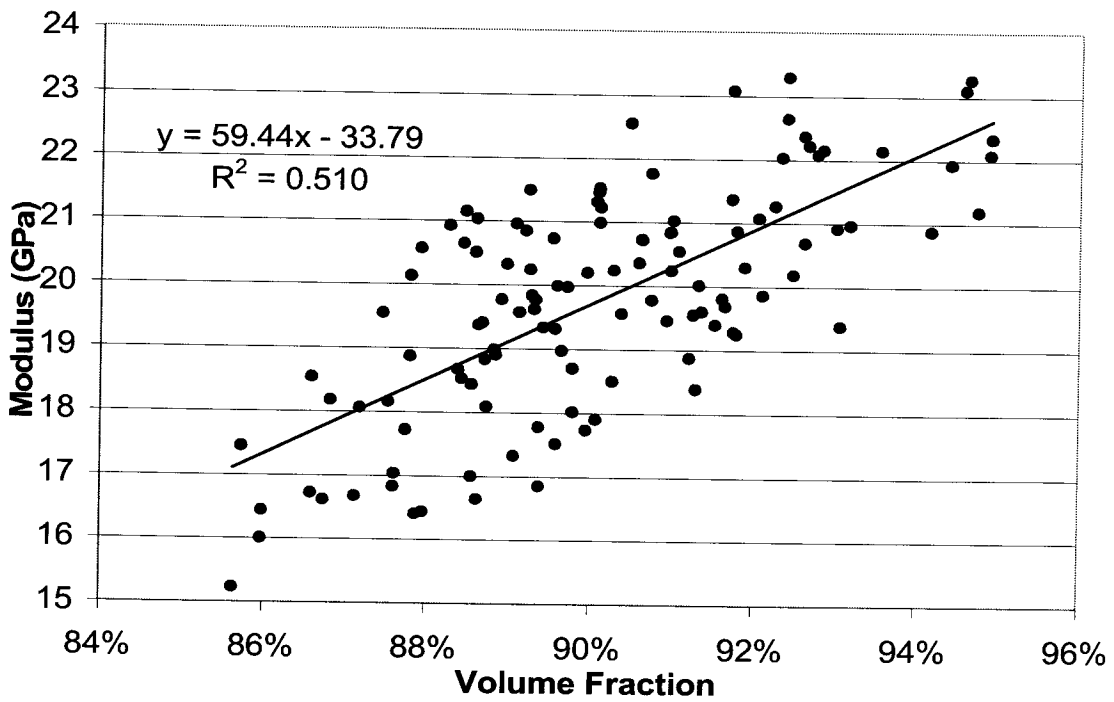


Figure 5-18 Linear regression for the correlation of elastic modulus and volume fraction of dentin in the transverse plane

The correlation coefficient for the regression of elastic modulus and volume fraction for dentin in the transverse plane is 0.71 with a p value of < 0.001 .

To determine whether or not both mineral content and volume fraction are explanatory variables that have independent effects on the elastic modulus of dentin in the transverse plane, a multiple linear regression was conducted using both variables. The correlation coefficient for this multiple linear regression was 0.73 ($R^2 = 0.527$) with a p value of < 0.001 .

5.2.3 Analysis of Jawbone

The elastic modulus of jawbone was measured using nanoindentation. The elastic modulus for 22 days old jawbone was measured to be 21.99 ± 1.88 GPa.

A scatterplot of elastic modulus versus mineral content for jawbone is presented in Figure 5-19. A linear regression for the correlation of elastic modulus and mineral content was calculated and presented in Figure 5-20.

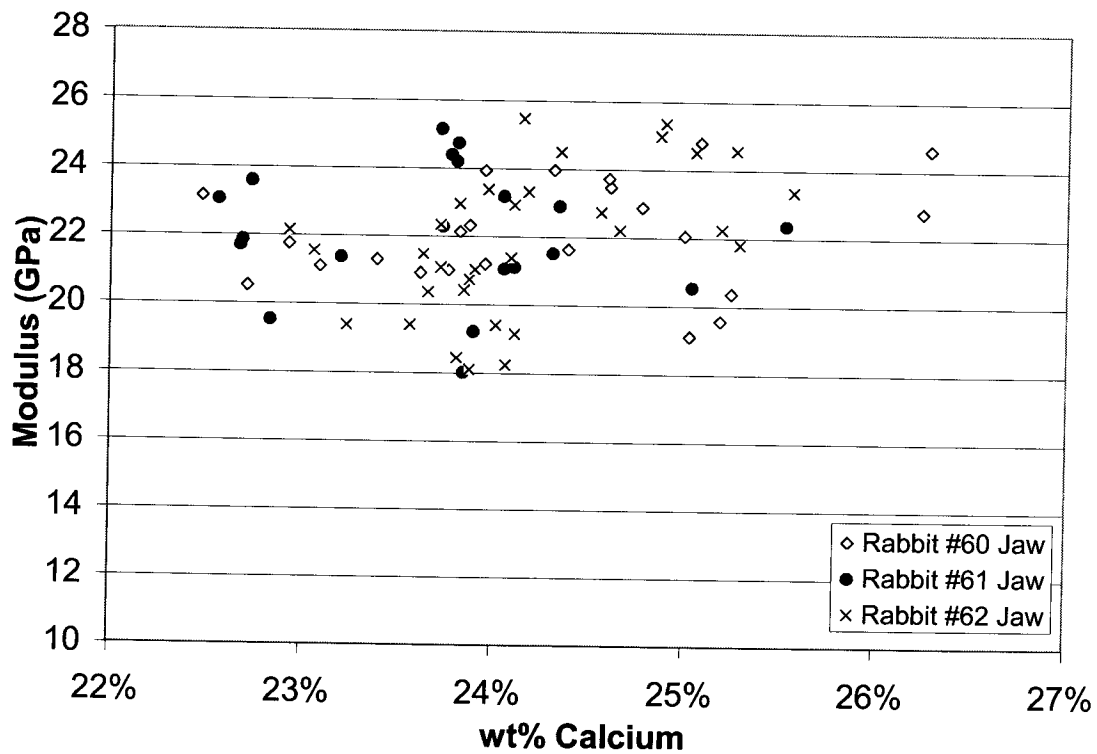


Figure 5-19 Scatterplot of elastic modulus vs. mineral content of jawbone

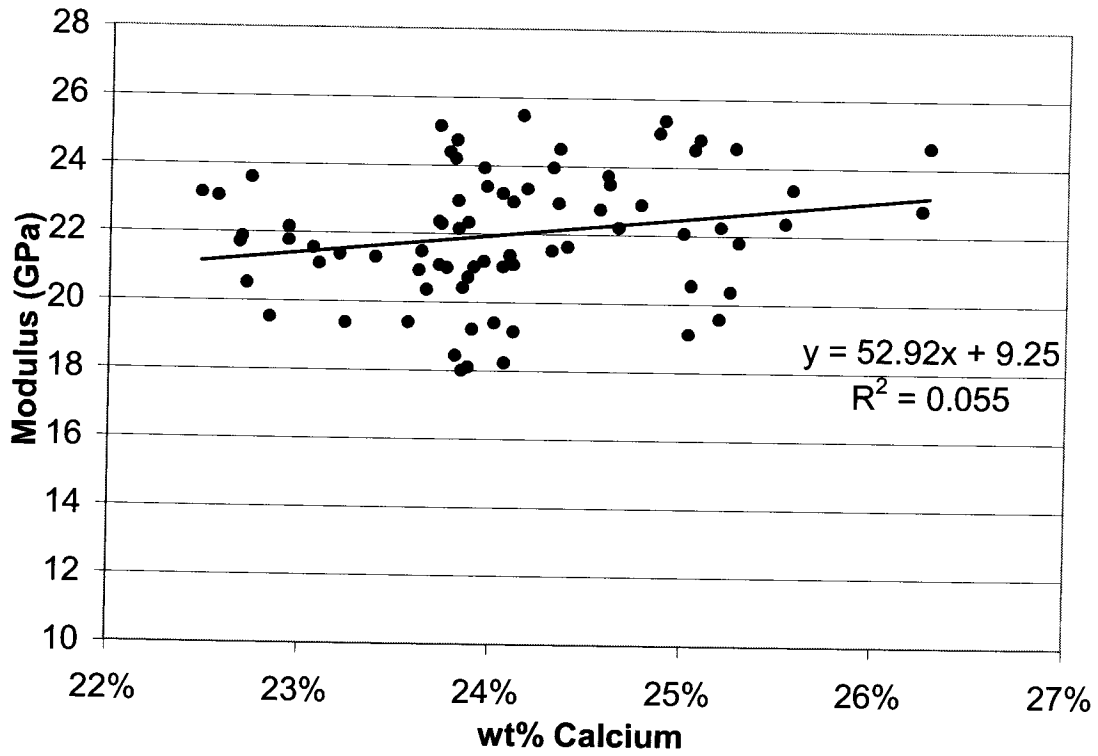


Figure 5-20 Linear regression for the correlation of elastic modulus and mineral content of jawbone

The correlation coefficient for the regression of elastic modulus and mineral for jawbone is 0.23 with a p value of < 0.001.

Chapter 6 Discussions

6.1 The Effects of Surface Coatings on the Elastic Modulus of Peri-Implant Bone

Many recent publications have reported the positive effects of hydroxyapatite on bone formation.^{11,72,73,74,75} These reports have found that a hydroxyapatite coating on orthopedic implants can increase ingrown bone volume and bone/implant contact lengths. Studies have also found that these improvements can be further amplified with the local delivery of bisphosphonate (alendronate is a form of bisphosphonate), an anti-osteoporosis drug believed to discourage the activities of osteoclasts (bone resorbing cells) while encouraging the activities of osteoblasts (bone forming cells). Although bone growth improvements are very important to the bone/implant fixation, another factor that needs to be considered is the mechanical properties of the coating/drug influenced bone. In this study, the elastic moduli of 15 days old peri-implant bone influenced by calcium phosphate coatings with or without alendronate were measured and compared. The elastic modulus of Ingrown Bone from calcium phosphate coated (Ta-CaP) implants were approximately 3 GPa higher than Ingrown Bone from the control (Ta) implant samples, and the difference was statistically significant. The elastic modulus of Ingrown Bone from calcium phosphate coating with alendronate (Ta-CaP-ALN) implants were also approximately 3 GPa higher than the Ingrown Bone bone from the control (Ta) implant samples, and the difference was also statistically significant. The elastic modulus difference between the Ingrown Bone from the two types of calcium phosphate coated samples (Ta-CaP and Ta-CaP-ALN) was minimal and not statistically significant.

Butz et al. reported that the surface roughness of implants alters biomechanical properties of bone integrated to implants. They reported that the elastic modulus of peri-implant bone from titanium implants with etched surfaces was 1.5 to 2.5 times higher than that of the un-etched control samples.⁴⁶ Since the calcium phosphate coating used in this study had a rougher surface than the bare Ta control implants¹¹, the results from Butz provides one possible explanation for the difference in elastic modulus between Ingrown Bone from Ta implants and the coated implants.

Another possible explanation can be derived from a strengthening mechanism proposed by Chen et al.⁷⁶ It is well established that the elastic modulus of bone is directly related to its mineral contents (wt% Ca).^{58,77} The mechanism proposed by Chen states that HA dissolves into the surrounding in-vivo solutions to form nanocrystallites precipitates in the collagen-matrix.⁷⁶ As a result, the mineralization rate of the corresponding bone could be influenced; therefore, the elastic modulus of the bone would also be influenced.

From the results gathered in this thesis, it is interesting to note that the addition of alendronate did not significantly increase the elastic modulus of Ingrown Bone. Anti-osteoporosis drugs such as alendronate are known to increase the mineralization rate of bone;^{78,79} however, the elastic modulus different between Ingrown Bone from Ta-CaP and Ta-CaP-ALN in this study was statistically insignificant. A possible explanation can be derived from the elastic modulus comparisons between Ingrown Bone and Host bone. The elastic modulus of Ingrown Bone from Ta-CaP implants and Ta-CaP-ALN were not

statistically different from their respective Host Bone; therefore, a possible explanation for the limited alendronate effect could be because the CaP coating alone increased the elastic modulus of Ingrown Bone to its biological maximum after 15 days of healing; thus, the addition of alendronate had a limited effect on the elastic modulus of Ingrown Bone.

From this thesis study the differences between the elastic moduli of Host Bone from the different implant groups were not statistically insignificant. This suggests that the effects of the CaP and CaP-ALN coatings on the elastic modulus of peri-implant bone are restricted to the Ingrown Bone only.

6.2 Effects of Mineral Content and Porosity on the Elastic Modulus of Dentin

The elastic modulus of dentin on the sagittal plane varies from the crown towards the root. A possible explanation could be that the volume fraction of intertubular dentin also increases in that pattern. This pattern corresponds with the elastic modulus data and the linear regression results also support this observation.

For this thesis, the properties of dentin from the anterior growth front on the transverse plane can be compared with the properties of dentin at approximately 40% to 50% of the length on the sagittal plane, since they are from approximately the same section (different plane) of the tooth. When comparing the modulus of dentin on both planes, the results suggest that the modulus is approximately 5 to 7 GPa higher on the transverse plane, while mineral content remain consistent approximately 25 to 26 Ca wt%. Volume fraction

is also fairly consistent, with a difference of approximately 2 to 4% between the two planes. A possible explanation for the difference in elastic modulus is the direction of the dentin tubules. On the sagittal plane, the tubules are perpendicular to the direction of the nanoindentations (applied load) while on the transverse plane the tubules are approximately parallel to the direction of the nanoindentations. This difference in tubules orientation may be a contributing factor for the elastic modulus difference.

Linear regression was used to determine the relationship between elastic modulus and mineral content, and elastic modulus and volume fraction on both the sagittal and transverse planes. The correlation coefficient (R value) of the relationship between elastic modulus and volume fraction was higher than the R value of the relationship between elastic modulus and mineral content. This observation was the same for data collected from both planes. This may suggest that volume fraction is the more influential variable. It is important to note, however, that this observation may be due to the limited Ca wt% range in dentin. Studies on bulk bone have shown that mineral content has the same influence if not more than that of volume fraction.^{58,80,81}

When both explanatory variables (mineral content and volume fraction) were applied to the linear regression model for elastic modulus, it was found that the correlation coefficient (R value) improved approximately by 0.02. This may or may not suggest that both of the variables have independent effects on the elastic modulus of dentin. Similar studies on bulk bone have shown that both mineral content and volume fraction have independent effects on the elastic modulus of bone.⁵⁸

In addition to the linear regressions presented in the results section, logarithmic regressions was also fitted to scatterplots to determine the relationship between elastic modulus and mineral content, and elastic modulus and volume fraction for dentin on both sagittal and transverse planes (Figure 6-1 to Figure 6-4).

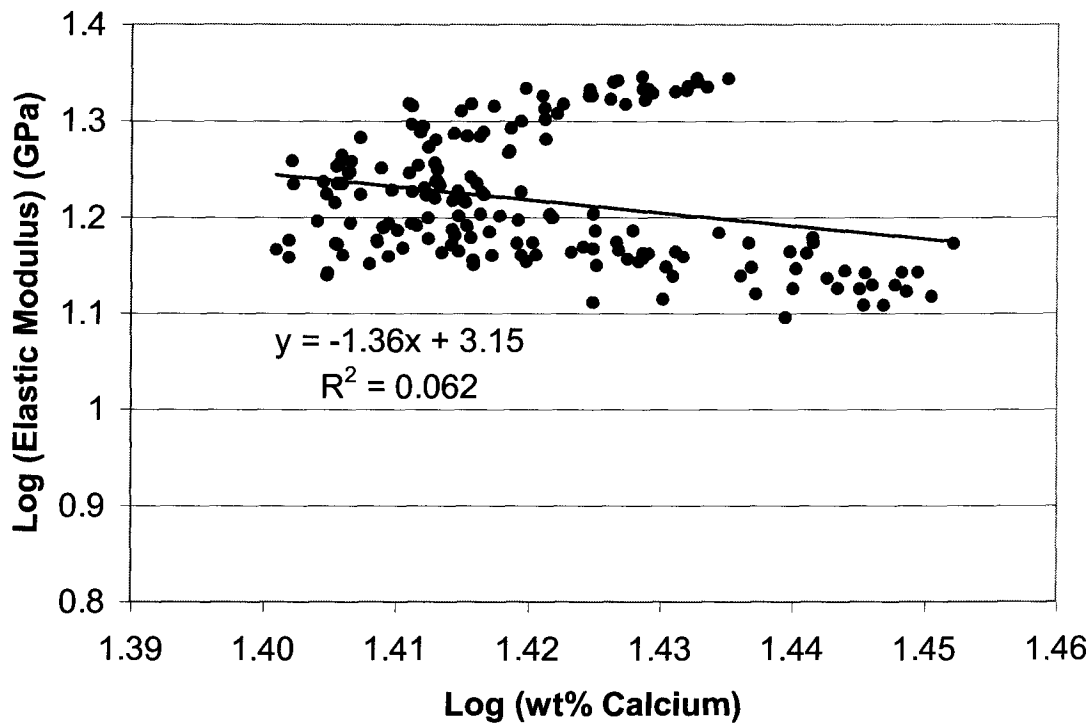


Figure 6-1 Logarithmic regression for the correlation between elastic modulus and mineral content of dentin in the sagittal plane

The correlation coefficient for the logarithmic regression of elastic modulus and mineral content for dentin in the sagittal plane is 0.248 with a p value of < 0.001 .

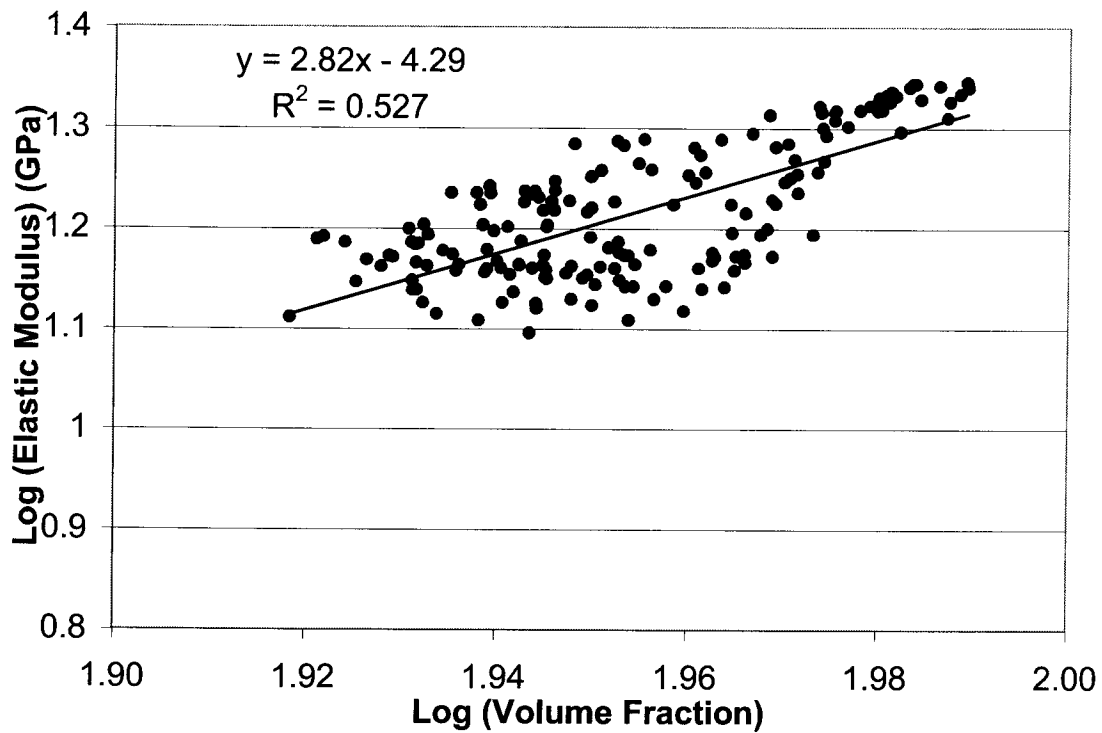


Figure 6-2 Logarithmic regression for the correlation of elastic modulus and volume fraction of dentin in the sagittal plane

The correlation coefficient for the logarithmic regression of elastic modulus and volume fraction for dentin in the sagittal plane is 0.73 with a p value of < 0.001.

A multiple logarithmic regression between elastic modulus and both variables (wt% Ca and volume fraction) yielded a correlation coefficient of 0.76 ($R^2 = 0.571$) with a p value of < 0.001.

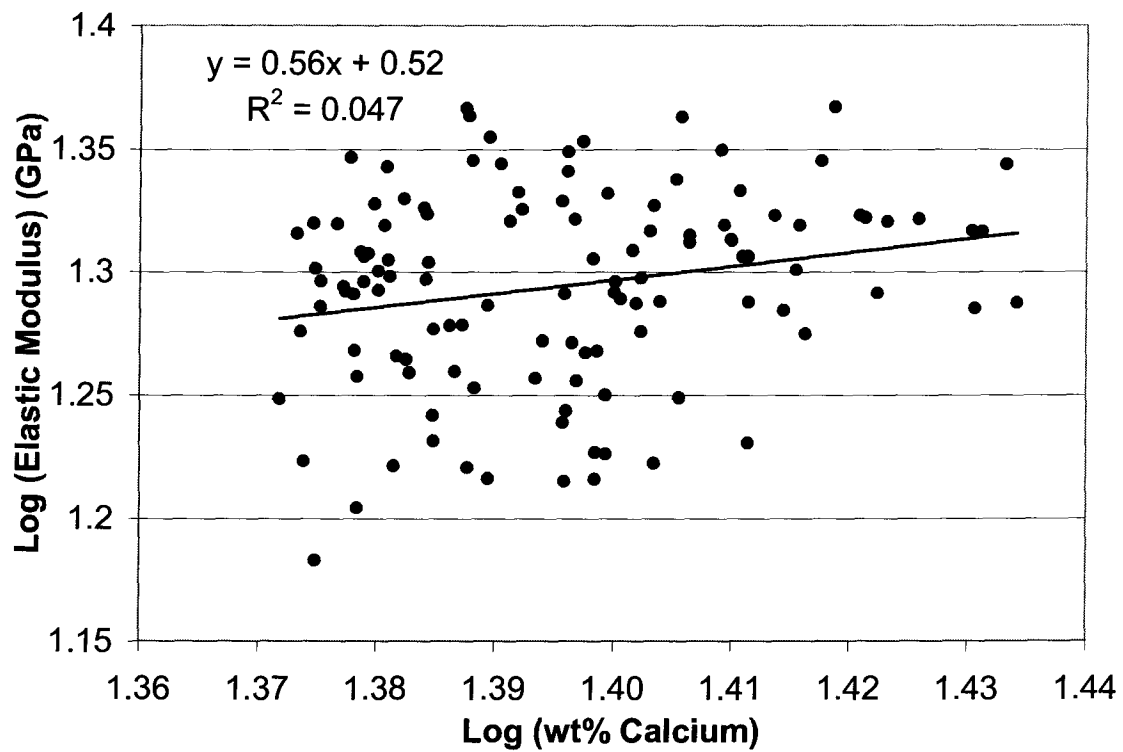


Figure 6-3 Logarithmic regression for the correlation of elastic modulus and mineral content of dentin on the transverse plane

The correlation coefficient for the logarithmic regression of elastic modulus and mineral content for dentin in the transverse plane is 0.22 with a p value of < 0.001.

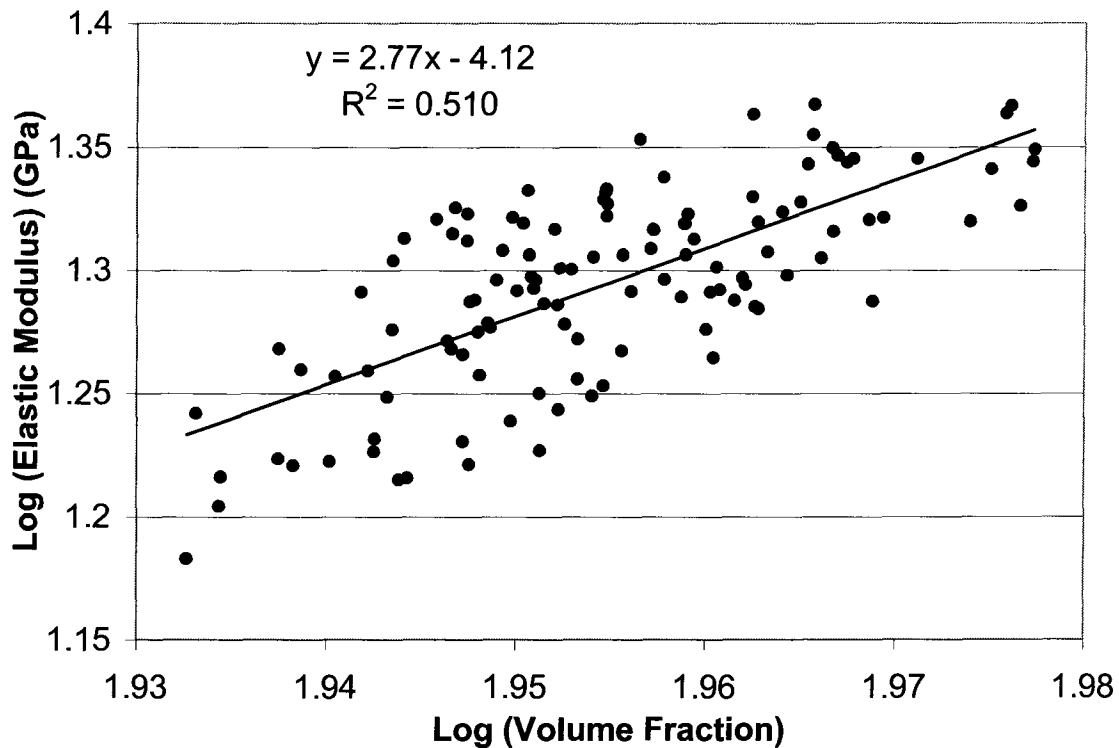


Figure 6-4 Logarithmic regression for the correlation of elastic modulus and volume fraction of dentin on the transverse plane

The correlation coefficient for the regression of elastic modulus and volume fraction for dentin on the transverse plane is 0.71 with a p value of < 0.001 .

A multiple logarithmic regression between elastic modulus and both variables (wt% Ca and volume fraction) yielded a correlation coefficient of 0.73 ($R^2 = 0.527$) with a p value of < 0.001 .

Studies investigating the properties of bone have demonstrated that logarithmic regressions of elastic modulus and mineral content, and of elastic modulus and volume fraction are better models than liner regressions for determining the relationship between

those properties. However, the data and regressions from this thesis study showed limited differences (R value difference of < 0.05) between linear and logarithmic models.

6.3 Difference between Dentin and Jawbone

An elastic modulus versus mineral content scatter plot of data from jawbone, dentin on the sagittal plane, and dentin on the transverse plane, is presented in Figure 6-5. From observations of the scatterplot, it suggests that jawbone has a higher modulus than dentin of the same age. This observation is supported by studies that have found similar results on dentin and bone from different species of animals.³⁰ The scatter plot also suggests that jawbone has a slightly lower mineral content.

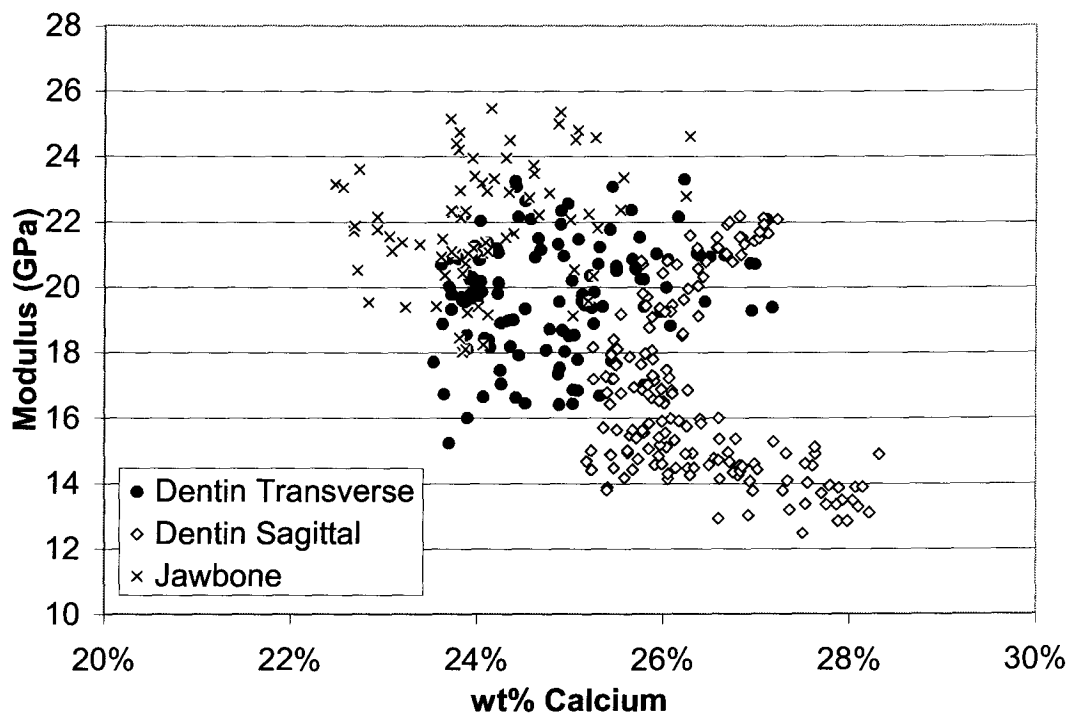


Figure 6-5 Elastic modulus vs. mineral content scatter plot of data from jawbone, dentin on the sagittal plane, and dentin on the transverse plane

Chapter 7 Conclusions

Peri-implant bone, dentin, and jawbone samples from rabbits were investigated. The following are the main conclusions drawn from the study.

1. The calcium phosphate coatings, with or without alendronate, on porous tantalum implants increased the elastic modulus of peri-implant Ingrown Bone by approximately 22% (3 GPa) when compared with Ingrown Bone from uncoated porous tantalum implants. The increase was statistically significant.
2. The addition of alendronate did not significantly increase the elastic modulus of peri-implant Ingrown Bone when the elastic modulus of the peri-implant Ingrown Bone from the Ta-CaP and Ta-CaP-ALN were compared.
3. The effects of calcium phosphate coatings, with or without alendronate, on the elastic modulus of peri-implant bone were local. The elastic modulus of the host trabecular bone was not significantly affected by the calcium phosphate coatings.
4. The elastic modulus of dentin is strongly dependent on the porosity and to a lesser extent on the calcium content. This was observed on both cross sectional planes.
5. When the properties of jawbone and dentin are compared, the elastic modulus of jawbone was generally higher than that of dentin while the mineral content was lower.

Chapter 8 Recommendations for Future Work

To establish further knowledge in the properties of peri-implant bone, dentin, and jawbone the following may be recommended for future studies:

- Apply the nanoindentation and quantitative backscattered electron imaging techniques to conduct a more in depth investigation on peri-implant bone, and correlated the elastic modulus with the bone mineral content.
- Systematic study on the effects of calcium phosphate coatings on peri-implant bone of different ages, and determine if alendronate has a significant effect on the elastic modulus of peri-implant bone of different ages.
- Apply the nanoindentation and quantitative backscattered electron imaging techniques to conduct an investigation on of peri-implant bone to include a comparison of bone of different ages.
- A more in depth study on the properties of dentin at different cross sections of the tooth. Include analyses on the effects of age, effects of tubular orientation, and conduct properties mapping across the entire plane of the tooth.

REFERENCES

- ¹ JC Wright, MC Weinstein, Gains in Life Expectancy from Medical Interventions – Standardizing Data on Outcomes, *N Engl J of Med*, 1998, 339, 6, 380-386
- ² Dental Implant and Bone Graft Markets to Approach \$3.5 Billion in 2010, Retrieved on Feb. 03 2008, *Medical News Today*, <http://www.medicalnewstoday.com/articles/29693.php>, 2005
- ³ L Waldegger, A Cranney, MMS Hing, D Coyle, Cost-Effectiveness of Hip Protectors in Institutional Dwelling Elderly, *Osteoporos Int*, 2003, 14, 243-250
- ⁴ Canadian Institute for Health Information (CIHI), 2006 Report Hip and Knee Replacements in Canada, 2006
- ⁵ W Tesch, N Eidelman, P Roschger, F Goldenberg, K Klaushofer, P. Fratzl, Graded Microstructure and Mechanical Properties of Human Crown Dentin, *Cal. Tis. Int.*, 2001, 69, 3, 147-157
- ⁶ A Gross, Report of the Total Hip and Knee Joint Replacement Expert Panel, 2005
- ⁷ M Tosto Jr., Dental Implants in Canada: A Growing Opportunity, *Oral Heal.*, 2006, 96, 8, 37-40
- ⁸ Dental Porous Titanium Foam Implants: An Idea with Bite, Retrieved on Feb. 03, 2008, National Research Council Canada, http://www.nrc-cnrc.gc.ca/highlights/2005/0507_titanium_implants-print_e.html, 2005
- ⁹ Dental Implants Benefits Replace Dentures and Bridges With Implant Dentistry, Retrieved on Feb. 03 2008, *Dental Resources*, <http://www.dental-resources.com/dental-implants.html>, 2006
- ¹⁰ K Duan, Bisphosphonate-Containing Coatings For Bone-Implants, PhD Thesis, U Brit Columbia, 2007
- ¹¹ Y Hu, Effects of Alendronate-Immobilized Calcium Phosphate Coating on Bone Growth into Porous Tantalum, M.A.Sc. Thesis, U. of Brit. Columbia, 2007
- ¹² H Denissen, C Montanari, R Martinetti, A van Lingen, A van den Hooff, Alveolar Bone Response to Submerged Bisphosphonate-Complexed Hydroxyapatite Implants, *J. Periodontology*, 2000, 71, 2, 279-286
- ¹³ S Meraw, CM Reeve, PC Wollan, Use of Alendronate in Peri-Implant Defect Regeneration, *J. Periodontol*, 1999, 70, 2, 151-158

- ¹⁴ M. Yoshinari, Y Oda, T Inoue, K Matsuzaka, M Shimono, Bone Response to Calcium Phosphate-Coated and Bisphosphonate-Immobilized Titanium Implants, *Biomaterials*, 2002, 23(14), 2879-2885
- ¹⁵ H Kajiwara, T Yamaza, M Yoshinari, T Goto, S Iyama, I Atsuta, MA Kido, T Tanaka, The Bisphosphonate Pamidronate on the Surface of Titanium Stimulates Bone Formation Around Tibial Implants in Rats, *Biomaterials*, 2005, 26(6), 581-587
- ¹⁶ R Wang, Anisotropic Fracture in Bovine Root and Coronal Dentin, *D. Mat.*, 2005, 21, 429-436
- ¹⁷ OL Harrysson, YA Hosni, JF Nayfeh, Custom-Designed Orthopedic Implants Evaluated Using Finite Element Analysis of Patient-Specific Computed Tomography Data: Femoral-Component Case Study, *BMC Muscu Dis*, 8, 2007, 91-101
- ¹⁸ History of Total Joint Replacement, Retrieved on Mar. 12 2008, Utah Hip and Knee Center, <http://www.utahhipandknee.com/history.htm>
- ¹⁹ M Windler, R Klabunde, Titanium for Hip and Knee Prostheses, in Brunette DM, P Tengvall, M Textor, Thomsen P ed. *Titanium in medicine*, p703-746, Springer, 2001
- ²⁰ Dr. Frank H. Gunston CM, Retrieved on Mar. 12 2008, University of Manitoba: Distinguished Graduates, <http://www.umanitoba.ca/honours/?s=gg&pg=ppl&det=39>
- ²¹ B Ratner, A History of Biomaterials, B Ratner, A Hoffman, F Schoen, J Lemons, *Biomaterials Science: An introduction to Materials in Medicine*, 10-19, Academic Press, 2004
- ²² P Lobo, H Edmonds, G Eden, Total Knee Replacement Multimedia Health Education, Your Practice Online
- ²³ T Albrektsson, A Wennerberg, The Impact of Oral Implants – Pass and Future, 1966-2042, *J. Can. Dent. Assoc.*, 2005, 71(5), 327a-d
- ²⁴ K Hebel, R Gajjar, T Hofstede, Single-Tooth Replacement: Bridge vs. Implant-Supported Restoration, *J Can Dent Assoc.*, 2000, 66, 435-438
- ²⁵ Endosseous Implants, Retrieved on Feb. 03 08, Implant Cosmetic Dental Center, http://maryland-implants.com/endosseous_implants.htm
- ²⁶ What Are Implants?, Retrieved on Feb. 03 08, Colgate Oral Care Information Check-ups & Dental Procedures, <http://www.colgate.com/app/Colgate/US/OC/Information/OralHealthBasics/CheckupsDentProc/DenturesAndDentalImplants/WhatAreImplants.cvsp>
- ²⁷ S Weiner, HD Wagner, The Material Bone: Structure-Mechanical Function Relations, *Annu. Rev. Mater. Sci.*, 1998, 28, 271-298

- ²⁸ JY Rho, L Kuhn-Spearing, P Zioupos, Mechanical Properties and the Hierarchical Structure of Bone, *Med. Eng. & Phys.*, 20, 2998, 92-102
- ²⁹ JH Kinney, SJ Marshall, GW Marshall, The Mechanical Properties of Human Dentin: A Critical Review and Re-Evaluation of The Dental Literature, *Crit Rev Oral Biol Med*, 14, 2003, 13-29
- ³⁰ JD Currey, *Bones Structure and Mechanics*, Princeton University Press, 2002, 175-193
- ³¹ H Bo, Z Quanshui, Effect of Dentine Tubules on the Mechanical Properties of Dentin. Part I: Stress-Strain Relations and Strength Criterion, *ACTA Mech Sinica (Eng Series)*, 15, 4, 1999, 355-365
- ³² JD Bobyn, SA Hacking, JJ Krygier, EJ Harvey, DG Little, M Tanzer, Zoledronic acid causes enhancement of bone growth into porous implants, *J. Bone Joint Surg. (Br)*, 2005, 87-B, 416-420
- ³³ JL Hay, GM Pharr, *Instrumented Indentation Testing*, Materials Park, OH: ASM International, 2000, 232-243
- ³⁴ MTS, *Theory of Instrumented Indentation Testing (IIT)*, Nano Indenter XP User's Manual, 27-38
- ³⁵ X Li, B Bhushan, A Review of Nanoindentation Continuous Stiffness Measurement Technique and its Applications, *Mat Char*, 48, 2002, 11-36
- ³⁶ WD Callister Jr, *Materials Science and Engineering: An Introduction*, 4 ed., John Wiley & Sons Inc, 1996, 109-146
- ³⁷ MR van Landingham, Review of Instrumented Indentation, *J Res Natl Inst Stand Technol* 108, 2003, 249-265
- ³⁸ L Silva, *Nanoindentation Study and Quantitative Backscattered Electron Imaging of Human Cortical Bone*, M.A.Sc. Thesis, U. of Brit. Columbia, 2006
- ³⁹ Nanoindentation, Retrieved on Mar 15 08, Wikipedia, <http://en.wikipedia.org/wiki/Nanoindentation>
- ⁴⁰ WC Oliver, GM Pharr, An Improved Technique for Determining Hardness and Elastic Modulus using Load and Displacement Sensing Indentation Experiments, *J Mater Res*, 7, 6, 1992, 1564-1583
- ⁴¹ A Fishcher-Cripps, *Nanoindentation* 2nd ed., Springer, NY, 2004, 39 - 68

- ⁴² JY Rho, ME Roy II, TY Tsui, GM Pharr, Elastic Properties of Microstructural Components of Human Bone Tissue as Measured by Nanoindentation, *J of Biomed Mat Res*, 45, 1999, 48-54
- ⁴³ JY Rho, TY Tsui, GM Pharr, Elastic Properties of Human Cortical and Trabecular Lamellar Bone Measured by Nanoindentation, *Biomater*, 18, 1997, 1325-1330
- ⁴⁴ JL Cuy, AB Mann, KJ Livi, MF Teaford, TP Weihs, Nanoindentation Mapping of the Mechanical Properties of Human Molar Tooth Enamel, *Arch Oral Bio*, 2002, 281-291
- ⁴⁵ QH Qin, MV Swain, A Micro-Mechanics Model of Dentin Mechanical Properties , *Biomater*, 25, 2004, 5081-5090
- ⁴⁶ F Butz, H Aita, CJ Wang, T Ogawa, Harder and Stiffer Bone Osseointegrated to Roughened Titanium, *J Dent Res* 85, 2006, 560-565
- ⁴⁷ ML Oyen, CC Ko, Examination of Local Variations in Viscous, Elastic, and Plastic Indentation Responses in Healing Bone, *J Mater Sci: Mater Med*, 18, 2007, 623-628
- ⁴⁸ L Saruwatari, H Aita, F Butz, HK Nakamura, J Ouyang, Y Yang, WA Chiou, T Ogawa, Osteoblasts Generate Harder, Stiffer and More Delamination-Resistant Mineralized Tissue on Titanium Than on Polystyrene, Associated With Distinct Tissue Micro- and Ultrastructure, *J Bone Min Res*, 20, 2005, 2002-2016
- ⁴⁹ A Kishen, U Ramamurty, A Asundi, Experimental Studies on the Nature of Property Gradients in the Human Dentine, *J Biomed Mat Res*, 51, 2000, 650-659
- ⁵⁰ P Roschger, H Plenck Jr, K Klaushofer, J Eschberger, A New Scanning Electron Microscopy Approach to the Quantification of Bone Mineral Distribution: Backscattered Electron Image Grey-Levels Correlated to Calcium $K\alpha$ -Line Intensities, *Scan Micro*, 9, 1995, 75-88
- ⁵¹ A Boyde, E Maconnachie, SA Reid, G Delling, GR Mundy, Scanning Electron Microscopy in Bone Pathology: Review of Methods, Potential and Applications, *Scan Elec Micro*, 6, 1986, 1537-1554
- ⁵² JL Goldstein, *Scanning Electron Microscopy and X-ray Microanalysis*, Kluwer Academic/Plenum, 3rd ed, 2003, 21-60
- ⁵³ RD Bloebaum, JG Skedros, EG Vajda, KN Bachus, BR Constantz, Determining Mineral Content Variations in Bone Using Backscattered Electron Imaging, *Bone*, 20, 1997, 485-490
- ⁵⁴ JG Skedros, RD Bloebaum, KN Bachus, TM Boyce, The Meaning of Graylevels in Backscattered Electron Images of Bone, *J Biomed Mater Res*, 27, 1993, 47-56

- ⁵⁵ TM Boyce, RD Bloebaum, KN Bachus, JG Skedros, Reproducible Methods for Calibrating the Backscattered Electron Signal for Quantitative Assessment of Mineral Content in Bone, *Scan Micro*, 4, 1990, 591-603
- ⁵⁶ L Angker, C Nockolds, MV Swain N Kilpatrick, Quantitative Analysis of the Mineral Content of Sound and Carious Primary Dentine using BSE Imaging, *J Arch Oral Bio*, 49, 2004, 99-107
- ⁵⁷ P Roschger, P Fratzl, J Eschberger, K Klaushofer, Validation of Quantitative Backscattered Electron Imaging for the Measurement of Mineral Density Distribution in Human Bone Biopsies, *Bone*, 23, 1998, 319-326
- ⁵⁸ JD Currey, The Effect of Porosity and Mineral Content on the Young's Modulus of Elasticity of Compact Bone, *J Biomechanics*, 21, 1988, 131-139
- ⁵⁹ SS Huga, WE Roberts, Mechanism of Osseointegration: Characterization of Supporting Bone with Indentation Testing and Backscattered Imaging, *Orthod*, 10, 2004, 162-173
- ⁶⁰ HS Gupta, S Schratte, W Tesch, P Roschger, A Berzlanovich, T Schoeberl, K Klaushofer, P Fratzl, Two Different Correlations Between Nanoindentation Modulus and Mineral Content in the Bone-Cartilage Interface, *J Struct Bio*, 149, 2005, 138-1478
- ⁶¹ M Weber, T Schoeberl, P Roschger, K Klaushofer, P Fratzl, Relating Local Bone Stiffness and Calcium Content by Combined Nanoindentation and Backscattered Electron Imaging, *Mat Res Soc Symp Proc*, 874, 2005
- ⁶² L Angker, C Nockolds, MV Swain N Kilpatrick, Correlating the Mechanical Properties to the Mineral Content of Carious Dentine-a Comparative Study Using an Ultra-micro Indentation System (UMIS) and SEM-BSE signals, *J Arch Oral Bio*, 49, 2004, 369-378
- ⁶³ RB Edwards, MJ Lopez, MD Markel, Histologic Analysis of Bone Healing, YH An, KL Martin, *Handbook of Histology Methods for Bone and Cartilage*, 375-390, Humana Press, 2003
- ⁶⁴ C Pautke, S Vogt, T Tischer, G Wexel, H Deppe, S Milz, M Schieker, A Kolk, Polychrome Labeling of Bone with Seven Different Fluorochromes: Enhancing Fluorochrome Discrimination by Spectral Image Analysis, *Bone*, 37, 2005, 441-445
- ⁶⁵ C Pautke, T Tischer, S Vogt, C Haczek, H Deppe, A Neff, HH Horch, M Schieker, A Kolk, New Advances in Fluorochrome Sequential Labelling of Teeth Using Seven Different Fluorochromes and Spectral Image Analysis, *J Anat*, 210, 2007, 117-121
- ⁶⁶ KH Frosch, I Sondergl, K Dresing, T Rudy, CH Lohmann, J Rabba, D Schild, J Breme, KM Stuermer, Autologous Osteoblasts Enhance Osseointegration of Porous Titanium Implants, *J Orth Res*, 2006, 213-223

- ⁶⁷ TW Bauer, D Mahovlic, Cutting and Grinding Methods for Hard-Tissue Histology, YH An, KL Martin, Handbook of Histology Methods for Bone and Cartilage, Humana Press, 2003, 233-242
- ⁶⁸ PK Zysset, XE Guo, CE Hoffler, KE More, SA Goldstein, Elastic Modulus and Hardness of Cortical and Trabecular Bone Lamellae Measured by Nanoindentation in the Human Femur, J of Biomech, 32, 1999, 1005-1012
- ⁶⁹ GX Ni, YS Choy, WW Lu, AHW Ngan, KY Chiu, ZY Li, B Tang, KDK Luk, Nano-mechanics of Bone and Bioactive Bone Cement Interfaces in a Load-Bearing Model, Biomaterials, 27, 2006, 1963-1970
- ⁷⁰ AK Bembey, ML Oyen, CC Ko, AJ Bushby, A Boyde, Elastic Modulus and Mineral Density of Dentine and Enamel in Natural Caries Lesions, MRS, 2005
- ⁷¹ SA Glantz, Primer of Biostatistics, McGraw-Hill Medical Publication Division, 6th ed, 2005, 73-125
- ⁷² W Suchanek, M yoshimura, Processing and Properties of Hydroxyapatite-based biomaterials for use as hard tissue replacement implants, J Mater Res, 13, 1998, 94-117
- ⁷³ G Willmann, Coating of Implants with Hydroxyapatite Material Connections Between Bone and Metal, Adv Eng Mater, 1, 1999, 95-105
- ⁷⁴ YL Chang, CM Stanford, JC Keller, Calcium and Phosphate Supplementation Promotes Bone cell Mineralization: Implications for Hydroxyapatite (HA)-enhanced bone formation, J Biomed Mater Res, 52, 2000, 270-278
- ⁷⁵ F Barrere, CM van der Valk, G Meijer, RAJ Dalmeijer, K de Groot, P Layrolle, Osteointegration of Biomimetic Apatite Coating Applied onto Dense and Porous Metal Implants in Femurs of Goats, J Biomed Mater Res, 67, 2003, 655-665
- ⁷⁶ QZ Chen, CT Wong, WW Lu, KMC Cheung, JCY Leong, KDK Luk, Strengthening Mechanisms of Bone bonding to Crystalline Hydroxyapatite in vivo, Biomater, 25, 2004, 4243-4254
- ⁷⁷ JD Currey, What Determines the Bendind Strength of Compact Bone, J Exp Biology, 202, 1999, 2495-2503
- ⁷⁸ W Yao, Z Cheng, KJ Koester, JW Ager, M Balooch, A Pham, S Chefo, C Busse, RO Ritchie, NE Lane, The degree of bone mineralization is maintained with single intravenous bisphosphonates in aged estrogen-deficient rats and is a strong predictor of bone strength, Bone, 41, 2007, 804 – 812

⁷⁹ DB Burr, L Miller, M Grynypas, J Li, A Boyde, T Mashiba, T Hirano, CC Johnston, Tissue mineralization is increased following 1 year treatment with high doses of bisphosphonates in dogs, *Bone*, 33, 2003, 960-969

⁸⁰ S Majumdar, HK Genant, S Grampp, DC Newitt, VH Truong, JC Lin, A Mathur, Correlation of Trabecular Bone Structure with age, Bone, Mineral Density, and Osteoporotic Status: In Vivo Studies in the Distal Radius Using High Resolution Magnetic Resonance Imaging, *J Bone Min Res*, 12, 1997, 111-118

⁸¹ G Evans, J Behiri, J Currey, W Bonfield, Microhardness and Young's modulus in cortical bone exhibiting a wide range of mineral volume fractions, and in bone analogue, *J Mat Sci: Mat in Med*, 1, 190, 38-43

APPENDIX

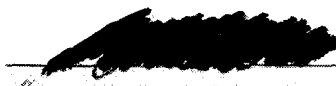
Ethical Approval for Animal Study

The University of British Columbia

ANIMAL CARE CERTIFICATE

PROTOCOL NUMBER: A04-0275	
INVESTIGATOR OR COURSE DIRECTOR:	Wang, R.
DEPARTMENT: Materials Engineering	
PROJECT OR COURSE TITLE: Calcium Bisphosphonate-Containing Composite Coating on Poreous Tantalum to Enhance Bone Ingrowth and Prevent Bone Resorption	
ANIMALS: Rabbits 36	
START DATE: 04-08-01	APPROVAL DATE: OCT 6 - 2004
FUNDING AGENCY: Zimmer Inc. (USA)	

The Animal Care Committee has examined and approved the use of animals for the above experimental project or teaching course, and have been given an assurance that the animals involved will be cared for in accordance with the principles contained in Care of Experimental Animals - A Guide for Canada, published by the Canadian Council on Animal Care.


Approval of the UBC Committee on Animal Care by one of:
Dr. W.K. Milson, Chair
Dr. J. Love, Director, Animal Care Centre
Ms. L. Macdonald, Manager, Animal Care Committee

This certificate is valid for one year from the above start or approval date (whichever is later) provided there is no change in the experimental procedures. Annual review is required by the CCAC and some granting agencies.

A copy of this certificate must be displayed in your animal facility.

Office of Research Services and Administration
102, Agronomy Road, Vancouver, V6T 1Z3
Phone: 604-827-5111 FAX: 604-822-6983